Fundamentals of SAR

Yaron Seliktar

Version - work in progress

© 2015 Yaron Seliktar
Permission is granted to copy, distribute and/or modify this document under the terms of the GNU Free Documentation License, Version 1.3 or any later version published by the Free Software Foundation; with no Invariant Sections, no Front-Cover Texts, and no Back-Cover Texts. A copy of the license is included in the section entitled "GNU Free Documentation License".

Chapter 1

Introduction

Synthetic Aperture Radar (SAR) is a radar that employs a *continuously displacing* (moving) aperture to create a *synthetically long aperture*, one that is much larger than the antenna's physical dimensions. SAR has traditionally been used in remote sensing applications for terrain *imaging* in *all weather conditions*. Other applications include:

- Target detection in dense foliage
- Surface displacement
- Surface parameter estimation
- Tomography using Polarimetric SAR

A classic and highly publicized example of SAR's capabilities is the mapping of planet Venus's surface by the Magellan probe. This was accomplished with a SAR/Altimeter combination. The SAR subsystem operated at 2.385 GHz and 325 W peak power, with range and cross-range resolution of 150 m [1]. It was able to peer through a dense $C0_2$ atmosphere, where optical equipment would be rendered useless. Some photos are shown in figure 1.1.

The primary application of SAR has been for terrain imaging and mapping. Other well known SAR modes are:

- *Differential SAR Interferometry* (DInSAR).
  An application of DInSAR is for *surface displacement measurements*, which can be used for earth-quake analysis, ground subsidence measurements and more.
- *Polarimetric SAR*
  This kind of SAR uses polarimetric SAR data to characterize surface type (wheat field, forest, surface minerals, etc.).
- *Combined Interferometry and Polarimetric SAR*
  This could be used for 3-D reconstruction of terrain or some other surface, otherwise known as Tomography.

1.1 Historical Overview

The precursor to SAR, Side-looking Aperture Radar (SLAR), was conceived in the 1950's [5]. It was recognized that instead of using a rotating antenna for azimuth coverage, an antenna

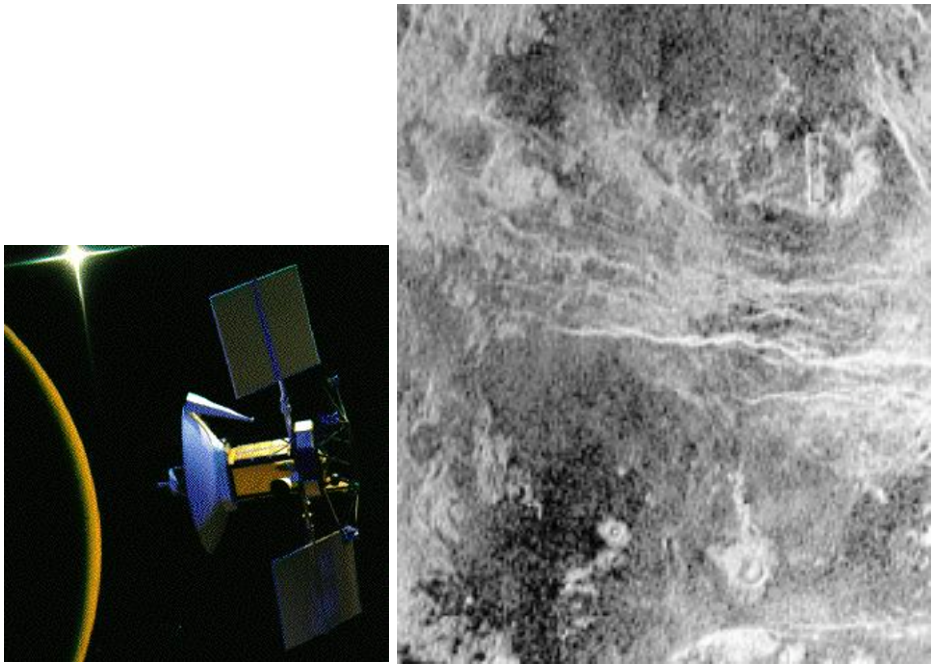

Figure 1.1: Magellan Probe (left). SAR Image (left). Photo Credits: NASA

could be fixed to the fuselage of an aircraft. The moving radar attains azimuth (or cross-range) coverage in this way. The sharper the beam is in azimuth, the better azimuth resolution is attained. A particularly high resolution imaging capability was attained by the AN/APQ-97 which utilized a pulse width much shorter than a micro-second and an operating frequency of 35 GHz that achieved a very narrow azimuth beam. A resolution of 10-20 meter was attained in both dimensions. SLAR attains along-track resolution merely by a narrow beam in azimuth and, therefore, makes no use of coherency [5].

In 1951 Carl Wiley, who at the time was employed by Goodyear Aircraft, described in a technical report a concept that he termed "Doppler Beam Sharpening" (DBS) [13]. The idea is to employ Doppler information on stationary targets for the purpose of increasing cross-range resolution [14].

In 1953 a team of researchers at the University of Michigan launched *Project Michigan* at the sponsorship of the U.S. Army Combat Surveillance Agency. It is in this setting that the idea of creating an extremely long "synthetic aperture" was conceived [6]. The first strip map was produced by Kovaly and co-workers of a section of Key West, Florida [9]. This early image did not employ pulse compression, nor was azimuth focused. However, despite the resulting low resolution nature of the strip map, it correctly depicted the water boundary, and other geometrical features of the scene being observed.

In 1958 Project Michigan produces the first focused SAR image of Fort Huachuca area and of Tucson, Arizona [6]. Digital recording techniques were not adequate at the time, and a recording that used photographic film was implemented. First operational airborne system – AN/UPD-1 ...

... Continue with Historical Overview

1.2 Literature

The literature is replete with material on SAR. General books on radar usually dedicate a chapter to SAR.

Recent years have seen a greatly expanded interest in SAR, and a tremendous growth of SAR technology and applications. With this came a plethora of literature dedicated to SAR. Both general books on SAR are available, as well those geared to a specific application or points of interest. Some books are geared more towards the engineer who is concerned with the hardware and data acquisition systems as well as the low-level signal processing, while others are geared more towards the image processing community who are concerned with producing images from both raw and processed SAR data.

In the evolution of SAR, certain landmark and key publications have come forth.

A book of compiled articles by John Kovaly, one of the leading engineers in the early development of SAR, can be found in [10]. The articles are categorized into 7 chapters, including a chapters on performance, processing and applications. He prefaces with a substantial introduction to SAR, and provides a short introduction to each chapter.

An early description of the work on SAR by the Michigan group led by Cutrona can be found in a 1961 article by Cutrona et al [6]. The authors begin with a brief theoretical framework of SAR and derive the optimal azimuth resolution. The authors proceed to present the efforts of the Michigan group in realizing a roof mounted prototype in 1953, followed in 1957 by a C-46F aircraft flown prototype SAR using optical processing. They also describe the development of the AN/UPD-1 and present accompanying high resolution SAR stripmaps obtained by this radar.

In a 1962 paper [12] by Sherwin[1] and other members of the group, the early development of SAR is presented. The paper begins with a summary of the theoretical work conducted by Wiley and some of his key contributions to SAR. The authors proceed to describe the Michigan group's independent work on SAR, detailing key properties of SAR as they were unfolded by Sherwin and others, such as the interpretation of SAR as a long synthetic array, and the use of focusing to achieve range independent resolution. The paper also provides stripmaps images produced in 1953.

In a mostly tutorial paper [2], Brown[2] examines SAR on a deeper level. For instance, he refrains from taking for granted such concepts as resolution and its commonly accepted definition as one over the bandwidth, but rather works with a more general definition, and illustrates how the accepted definition derives from it. He also justifies why resolution is a more effective performance criteria in imaging than, say, mean-square-error analysis. The paper begins with a CW analysis of SAR (single range bin), followed by a derivation of the optimal matched filter. It then proceeds to extend the theory to pulsed SAR (multiple range bins) and resulting ambiguities. Optical processing is considered next as a suitable implementation of the image processor. A natural extension of the theory is that of "imaging of a rotating target field", more commonly known as *Inverse Synthetic Aperture Radar (ISAR)*. The paper finalizes with a thorough treatment of phase errors, culminating with an expression that relates mean-square resolution to the phase-error spectrum and applied taper.

An excellent 1969 tutorial paper by Brown and Porcello [3] provides a thorough overview of SAR. It begins with a theoretical overview of SAR (including ISAR). It highlights the difference between *focused* and *unfocused* SAR, and describes optical processing. ...

A 1972 paper by Kovaly [9] introduces the idea of employing a space-borne SAR for high resolution planetary mapping. He begins by noting a 1964 paper [11] that describes a preliminary design of a radar system for mapping Venus by an orbiting spacecraft aimed at achieving a

[1] Michigan group director.

[2] At the time of writing he headed the Radar and Optics Lab at the University of Michigan, Ann Arbor.

resolution of 15-20 kilometers using conventional radar techniques. He then proceeds to elaborate on employing a SAR system in place of the conventional radar to obtain high resolution imagery of planetary terrain. Although the author provides a good overview of SAR principles it doesn't specifically address technological challenges that arise in a space-borne implementation.

A 1982 36 page article by Elachi [7] provides a comprehensive overview of *spaceborne* SAR, and issues pertinent to SAR when deployed in space. He begins with spaceborne SAR principles, in which he treats among other things, ambiguities, and the effects of *range migration*[3], effects of the Earth's rotation, orbit ellipticity, and space-craft attitude errors in the point target response. He also addresses technological factors in the implementation and signal processing of spaceborne SAR. The three satellite based SAR systems that had been deployed till that time Seasat SAR, Shuttle Imaging Radar-A (SIR-A), Apollo Lunar Sounder (ALSE)[4], are documented in the article, with particular emphasis on Seasat.

A short book by J. Patrick Fitch titled *Synthetic Aperture Radar* [8] serves as a good introduction to SAR. The author has in mind a cross-disciplinary audience, and as such, dedicates a chapter and appendix to Radar and signal processing fundamentals, as pertains to SAR processing. He provides an intuitive, yet mathematically rigorous treatment of the topics he addresses. A particularly noteworthy feature of the book, is the description of the SAR processor software (with included pseudo-FORTRAN code) as implemented for the Seasat mission. The book also has an excellent treatment of optical SAR processing.

A highly recommended book by Curlander and McDonough entitled *Synthetic Aperture Radar: Systems and Signal Processing* [5] provides a comprehensive treatment of SAR, which includes basic theory, imaging algorithms, SAR flight system, SAR ground system, and SAR data calibration.

Continue with other books...

[3]Range migration includes both range curvature and range walk [7].

[4]The ALSE was used for subsurface sounding of the lunar crust, rather than for surface imaging [7].

Chapter 2

SAR Basics

2.1 SAR Modes

SAR has three principal modes of illumination [4]:

- Stripmap
- Spotlight
- Scan

The basic method of illumination for each mode is illustrated in figure 2.1. The distinction between these modes is in the manner in which the terrain is illuminated. In stripmap SAR, the aperture beam can be either broadside (broadside stripmap), as illustrated in the figure, or squinted (squinted stripmap). In the stripmap mode the beam direction stays fixed with respect to the the aircraft. As such, an elongated strip of terrain is illuminated during the observation interval.

In spotlight SAR the beam direction is continuously rotated, so as to illuminate the same patch of terrain. The advantage of spotlight mode is the finer azimuth resolution that is attained.

Stripmap mode is utilized when wide swaths of terrain are to be mapped at reduced azimuthal resolution. Spotlight mode is utilized when localized swaths of terrain are to be mapped at finer azimuthal resolution.

Scan SAR is the most versatile mode, allowing arbitrary stretches of terrain to be illuminated. Because of the complexity of both the scanning mechanism and post-processing, scan SAR is not as commonly implemented as the other modes.

2.2 SAR Geometry

In order to discuss what happens in a SAR system, it is necessary to understand the geometry of the SAR system with respect to the terrain being mapped, as well as define geometrical quantities that will be used to formulate and quantify SAR behavior. For the sake of simplicity, *broadside stripmap* SAR and a flat Earth are initially assumed. An analysis of a SAR system based on the flat Earth approximation is sufficiently accurate for sensors carried aboard an aircraft. Analysis of an artificial-satellite based sensor, a topic that will be dealt with further on, requires a curved Earth model.

The simplified geometry is illustrated in figure 2.2.

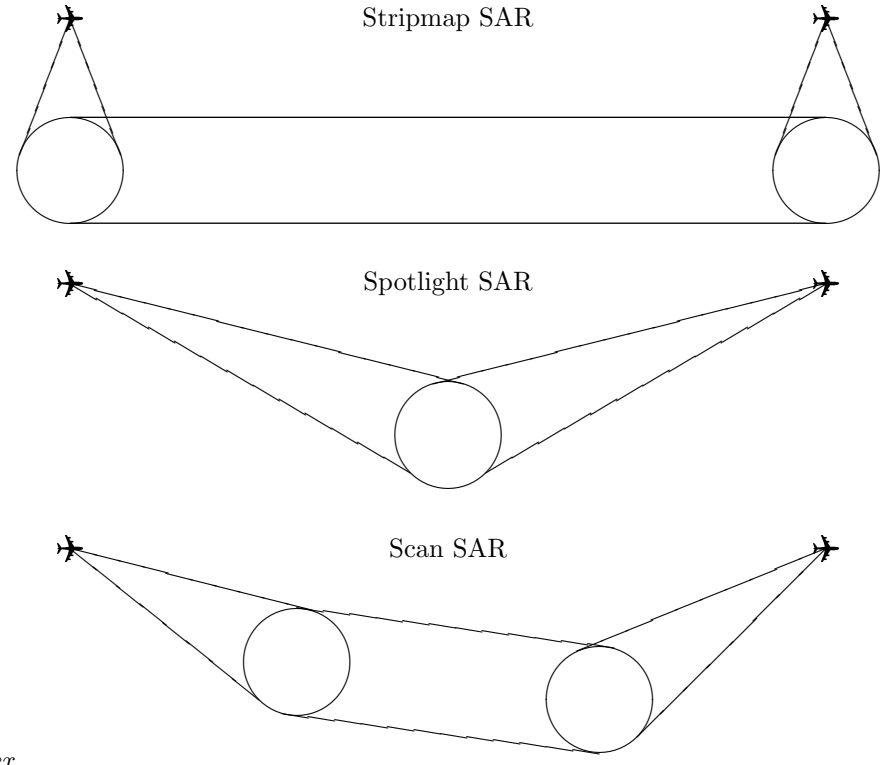

sarilluminationmodes.tex

Figure 2.1: The three conventional SAR modes.

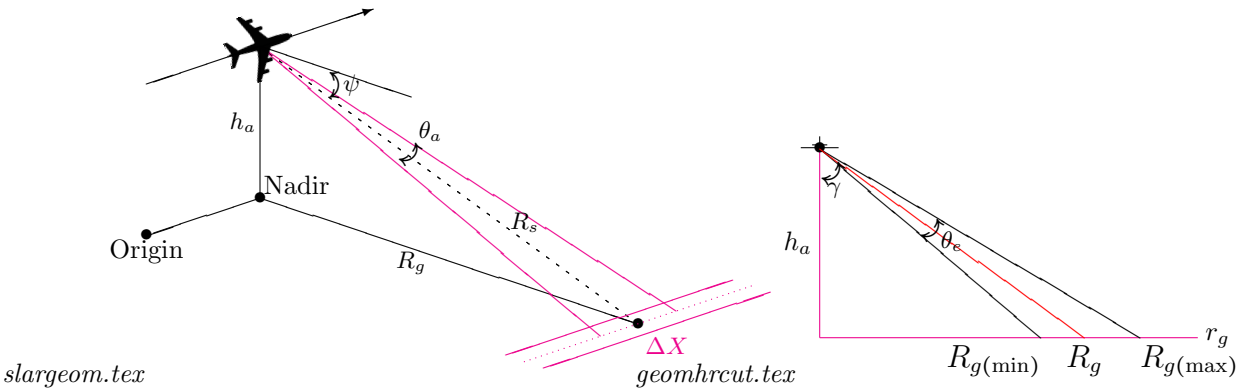

slargeom.tex *geomhrcut.tex*

Figure 2.2: Basic SAR geometry (left). A cut in cross-range (right).

- The *sensor path* is parallel to the Earth in the direction of flight, at height h_a above *nadir*.
- *Nadir* is the point on the ground nearest the aircraft. For the flat Earth geometry the line connecting nadir and the aircraft is orthogonal to the ground.
- The number of pulses transmitted is denoted M_{dat}
- The time interval over which data is collected is denoted T_{dat}
- The aperture beamwidth in both azimuth and elevation are denoted θ_a and θ_e, respectively.
- The *beam footprint* is the patch of terrain illuminated by the mainlobe of the physical aperture. The mainlobe is bounded by the azimuth and elevation beamwidths.
- The LOS is a line connecting the center of the aperture to the *target*. Since the LOS moves together with the aircraft, it is a function of time. The magnitude of the LOS is known as *slant range*, and denoted R_s, The unit vector in that direction may be denoted $\hat{R}_s$.
- The target in SAR is a hypothetical point on the terrain that will eventually correspond to a *pixel* in the pulse-compressed image. Unlike with conventional radar, where the terrain is generally considered clutter, and the more it is suppressed, the better, in SAR both background terrain and outstanding objects factor in as targets. Different regions of the terrain and objects exhibit differing degrees of electro-magnetic reflection, and that determines how bright a given patch of terrain or object will appear in the processed SAR image.
- The projection of the slant range vector onto the ground is denoted $\vec{R}_g$. Its magnitude, denoted R_g, is the *ground range*.
- The depression angle is ψ. For the flat Earth geometry being assumed the angle between the ground and LOS, known as the *grazing angle*, is also ψ. This is a valid assumption for some airborne SARs, but not for spaceborne SAR.
- The angle between the axis labeled h_a and the LOS is called the *look angle* and denoted γ. Note, for the simplified geometry presented $\gamma = 90° - \psi$.

2.2.1 Slant range, ground range and range resolution

With these definitions it is now possible to obtain the minimum and maximum slant range:

$$R_{s(\min)} = \frac{h_a}{\cos(\gamma - \theta_e/2)}, \qquad R_{s(\max)} = \frac{h_a}{\cos(\gamma + \theta_e/2)}$$

The corresponding ground ranges are:

$$R_{g(\min)} = h_a \tan(\gamma - \theta_e/2), \qquad R_{g(\max)} = h_a \tan(\gamma + \theta_e/2)$$

The slant range to the center of the footprint is:

$$R_s = \frac{h_a}{\cos(\gamma)}$$

The resolution in slant range is:

$$\Delta R_s = \frac{c\tau}{2}$$

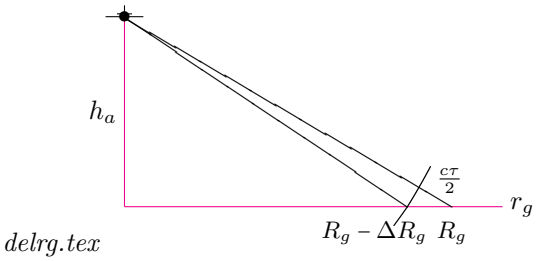

delrg.tex

Figure 2.3: Range resolution.

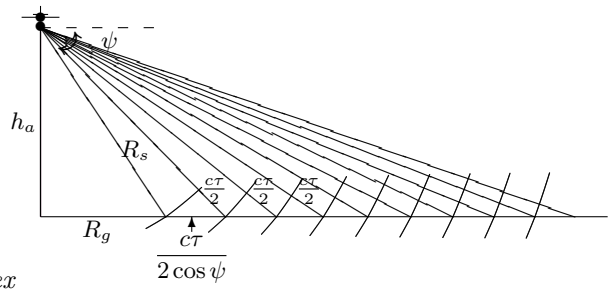

slargeomsideview.tex

Figure 2.4: SLAR - side view.

Since the direction of propagation is in the direction of the slant, the range resolution in that direction is independent of range.

The ground range resolution, ΔR_g, on the other hand is range dependent. The geometry used to derive an expression for ΔR_g is depicted in figure 2.3. By definition the circular wavefront radiating from the source antenna is perpendicular to both slant range lines. However, since the separation between slant range lines is small, the curved wavefront shown cutting through the two slant ranges can be approximated as a straight line, making a right angle with the longer slant range. Furthermore, assuming a flat Earth geometry, the grazing angle is merely the depression angle, ψ. Thus, the side adjacent to ψ is $c\tau/2$ and the hypotenuse is ΔR_g, and therefore:

$$\cos(\psi) \approx \frac{c\tau/2}{\Delta R_g}$$

Solving for range resolution:

$$\Delta R_g \approx \frac{c\tau}{2}\sec(\psi) = \Delta R_s \sec(\psi)$$

Clearly, ground range resolution decreases with range, asymptotically approaching that of slant range

$$\Delta R_s = \frac{c\tau}{2}$$

as ψ approaches zero. This is further illustrated in figure 2.4.

Since unprocessed SAR data is based on slant range geometry, the nonlinear relationship between slant range and ground range has to be accounted for when constructing an image from the SAR data in (rectangular) Earth coordinates.

2.2.2 Cross-Range

In discussing SAR, the azimuth dimension is typically referred to as *cross-range*. We first consider a conventional side-looking aperture radar (SLAR). In SLAR, the antenna broadside is perpendicular to the flight path. The *cross-range resolution* is range-dependent and expressed as:

$$\Delta x \approx \theta_a R_s$$

We now wish to relate the cross-range resolution to antenna dimensions and operating wavelength.

For a real planar antenna operating at the diffraction limit, the peak gain and antenna area, A, are related to each other by:

$$G = \frac{4\pi A}{\lambda^2} = \frac{4\pi L_a L_e}{\lambda^2}$$

In the second equality, the area is expressed as the product of L_a and L_e – the horizontal (azimuthal) and vertical (elevation) dimensions of the antenna, respectively.

Another relation governing peak gain is:

$$G \propto \frac{4\pi}{\theta_a \theta_e}$$

Equating the two expressions:

$$\frac{4\pi L_a L_e}{\lambda^2} = \frac{4\pi}{\theta_a \theta_e} \quad \Rightarrow \theta_a \theta_e = \frac{\lambda^2}{L_a L_e}$$

For a rectangular antenna the azimuthal and elevation beamwidths are independent, and can therefore be separated as follows:

$$\theta_a = \frac{\lambda}{L_a}, \quad \theta_e = \frac{\lambda}{L_e} \tag{2.1}$$

Substituting back into the expression for cross-range resolution, we have:

$$\Delta X \approx \theta_a R_s = \frac{\lambda}{L_a} R_s$$

From this expression we conclude that cross-range resolution is proportional to *wavelength* and *range*, and inversely proportional to *antenna length*.

2.2.3 Synthetic Antenna

Next we consider a synthetic antenna. A synthetic antenna is created when a real antenna traverses a distance L_s, intermittently transmitting pulses, and the rest of the time listening for echoes. The distance of travel between pulse transmission is akin to the inter-element spacing of a phased array.

The half-power beamwidth of a horizontally oriented linear untapered phased-array is:

$$\theta_a = \frac{\lambda}{L}$$

where L is the array length. For a synthetic array of synthetic length L_s, the beamwidth is:

$$\theta_s = \frac{1}{2} \frac{\lambda}{L_s} \tag{2.2}$$

The factor of a "half" can be explained as follows. In a real array phase shifts during transmission affect the direction in which energy is transmitted, but have no bearing on the spatial coherency of the returns, and therefore on the radiation pattern at receive. In contrast, in a synthetic array, phase-shifts on both transmission and reception have bearing on the spatial coherency of the returns, and are, therefore, both factored into the effective radiation pattern.

Concerning a single target, the length of the synthetic array is the distance the aircraft travels with the target contained within its beamwidth. This distance is range dependent and equal to:

$$L_s = \theta_a R_s = \frac{\lambda}{L_a} R_s \tag{2.3}$$

The second equality substituted for beamwidth as taken from equation 2.1.

The cross-range resolution of the synthetic aperture is thus:

$$\begin{aligned} \Delta X_s &= \theta_s R_s \\ &= \frac{1}{2}\frac{\lambda}{L_s} R_s \\ &= \frac{1}{2}\frac{\lambda}{\frac{\lambda}{L_a}} R_s \\ &= \frac{1}{2} L_a \end{aligned}$$

The second line substitutes for synthetic beamwidth as taken from equation 2.2. The third line substitutes for synthetic aperture length as taken from equation 2.3. The result demonstrates that cross-range resolution is governed solely by the aperture length of the on-board antenna, and is not range dependent, as is the case with a real antenna.

In fact, the smaller the antenna the better the cross-range resolution. This last fact is a bit misleading, since a smaller antenna results in a larger half power beamwidth, which means the plane traverses a larger distance with the target in its view. So indeed, the resolution is improved, but at the expense of a longer observation interval. There is a further limitation on resolution that will be considered in a more detailed analysis to follow.

Example 1

The following example illustrates some of the SAR concepts covered thus far. As additional theory is presented the example will be extended to cover additional aspects as well.

Considered is an air-borne strip-mode SAR flying at a height of 1 km. The antenna is 1 meter by 1 meter, and transmits at a center frequency of 10 GHz. The antenna is side-looking with boresight positioned at a 10° depression angle. The transmitted waveform is LFM with a compressed pulse width of 10 nS.

- Determine both slant and ground ranges at the center of the beam as well as the extremities.
- Determine both slant and ground resolution at the center of the beam and extremities.
- Determine the cross-range resolution of a conventional SLAR at the beam center.
- Determine the theoretical cross-range resolution.
- Sketch a cut in cross-range of the flight geometry and illuminated patch.

Solution
The wavelength is:

$$\lambda = c/f_c = \frac{3 \times 10^8 \text{ m/s}}{10 \text{ GHz}} = 0.03 \text{ m}$$

The look angle is:

$$\gamma = 90^\circ - \psi = 90^\circ - 10^\circ = 80^\circ$$

The azimuthal beamwidth is:

$$\theta_a = \frac{\lambda}{L_a} = \frac{0.03 \text{ m}}{1 \text{ m}} = 0.03 \text{ rad} = 1.7189^\circ$$

Slant range at center and extremities of footprint are:

$$\begin{aligned} R_s &= \frac{h_a}{\cos(\gamma)} = \frac{1 \text{ km}}{\cos(80^\circ)} = 5.759 \text{ km} \\ R_{s(\min)} &= \frac{h_a}{\cos(\gamma - \theta_e/2)} = \frac{1 \text{ km}}{\cos(80^\circ - 1.7189^\circ)} = 5.308 \text{ km} \\ R_{s(\max)} &= \frac{h_a}{\cos(\gamma + \theta_e/2+)} = \frac{1 \text{ km}}{\cos(80^\circ + 1.7189^\circ)} = 6.295 \text{ km} \end{aligned}$$

Ground range at center and extremities of footprint are:

$$\begin{aligned} R_g &= h_a \tan(\gamma) = (1 \text{ km}) \tan(80^\circ) = 5.671 \text{ km} \\ R_{g(\min)} &= h_a \tan(\gamma - \theta_e/2) = (1 \text{ km}) \tan(80^\circ - 1.7189^\circ/2) = 5.213 \text{ km} \\ R_{g(\max)} &= h_a \tan(\gamma + \theta_e/2) = (1 \text{ km}) \tan(80^\circ + 1.7189^\circ/2) = 6.215 \text{ km} \end{aligned}$$

Slant range resolution is independent of the position within the beam:

$$\Delta R_s = \frac{c\tau}{2} = \frac{3 \times 10^8 \text{ m/s}(10 \text{ nS})}{2} = 1.5 \text{ m}$$

Ground range is:

$$\begin{aligned} \Delta R_g &\approx \frac{c\tau}{2} \sec(\psi) = \Delta R_s \sec(\psi) = (15 \text{ m}) \sec(10^\circ) = 15.231 \text{ m} \\ \Delta R_{g(\min)} &\approx \Delta R_s \sec(\psi - \theta_e/2) = (15 \text{ m}) \sec(10^\circ - 1.7189^\circ/2) = 15.193 \text{ m} \\ \Delta R_{g(\max)} &\approx \Delta R_s \sec(\psi + \theta_e/2) = (15 \text{ m}) \sec(10^\circ + 1.7189^\circ/2) = 15.274 \text{ m} \end{aligned}$$

The cross-range resolution of a conventional SLAR at the center of the beam is

$$\Delta X = \theta_a R_s = (0.03 \text{ rad})(5.759 \text{ km}) = 172.7 \text{ m}$$

The theoretical cross-range resolution is

$$\Delta X_s = \frac{1}{2} L_a = \frac{1}{2}(1 \text{ m}) = \frac{1}{2} \text{ m}$$

and is independent of the beam position.
The cross-range cut is shown in figure 2.5.

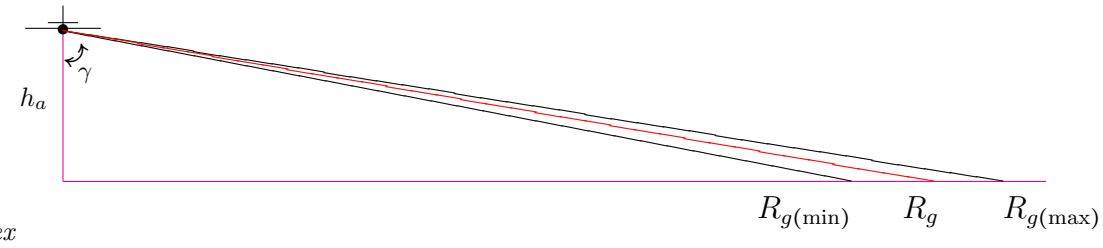

eg1geom.tex

Figure 2.5: Cross-range cut of geometry in example 1.

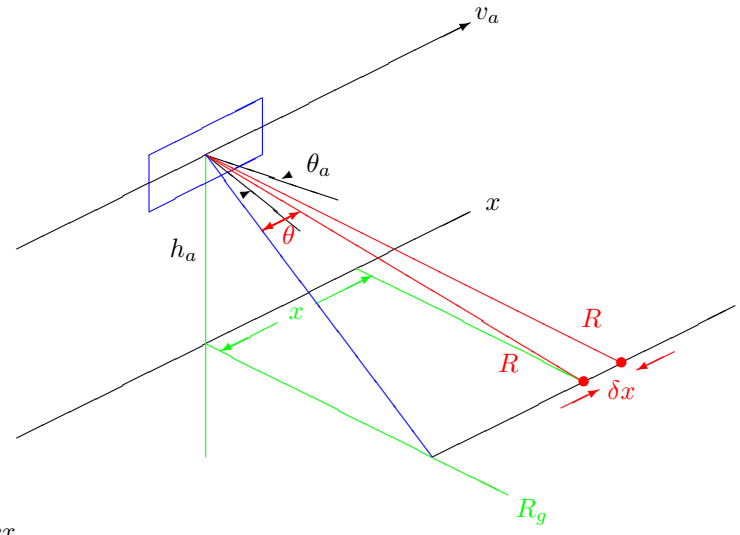

offbroadsidescatres.tex

Figure 2.6: Illumination geometry for two off-broadside scatterers.

2.3 Relationship Between Doppler Shift and Cross-Range

In the previous analysis it was claimed that SAR can achieve enhanced cross-range resolution with a theoretical limit of $L_a/2$. We now proceed to demonstrate the connection between cross-range and Doppler shift, and how this limit on cross-range resolution is obtained.

Consider two off-broadside scatterers within the illuminated swath that are captured by the radar beam, as illustrated in figure 2.6. The two scatterers are indicated in the figure by two small filled circles. The cross-range resolution, δx, is defined as the minimum separation between the scatterers for which the radar can distinguish between them. For simplicity, the aircraft velocity is assumed perpendicular to antenna broadside, in which case there are no velocity components in the y and z direction.[1] The aircraft speed is denoted v_a. For a flat Earth approximation the relative velocity between a scatterer and aircraft is also v_a.

Next, consider one of the off-broadside scatterers, as illustrated in figure 2.7. Its cross-range coordinate is denoted x. Since the aircraft is in motion relative to the scatterer a Doppler shift

[1] This assumption is approximately valid under mild winds conditions. A more general treatment, however, would consider other velocity components imposed on the aircraft.

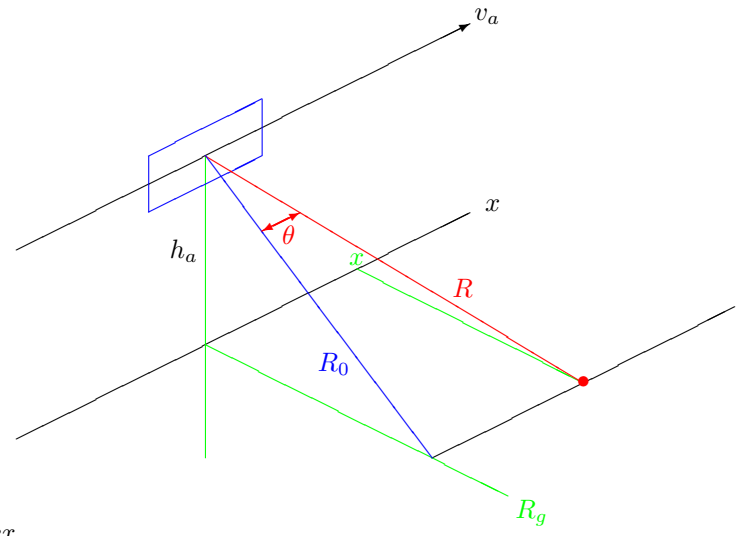

offbroadsidescat.tex

Figure 2.7: Illumination geometry for a single off-broadside scatterer.

is incurred for any off-broadside scatterer, given by

$$f_D = \frac{2v_a \sin(\theta)}{\lambda} = \frac{2v_a x}{R\lambda} \tag{2.4}$$

where $\sin(\theta) = x/R$ was used to obtain the second equality.

The cross-range coordinate of the scatterer, x, can, thus, be obtained from the Doppler

$$x = \frac{R\lambda}{2v_a} f_D \tag{2.5}$$

Since scatterers with slightly varying angles produce slightly varying Dopplers, they appear distinguished on a slow-time[2] spectrogram.

This is illustrated in figure 2.8. In this example, an aircraft flying at 100 m/s transmitting at wavelength 0.03 m, transmits 1000 pulses at a PRF of 2000 Hz. Three scatterers (with a one degree tapered spread) were placed at slant range 10 km and angles −7, −2 and +4.5 degrees relative to boresight. Their Dopplers were calculated using equation 2.4, and 1000 raw samples were generated for the range gate corresponding to 10 km. The spectrogram shown in the figure is the DFT of those samples. Equation 2.5 can be used to map between the Doppler frequencies where the peaks on the spectrogram occur and the corresponding cross-range coordinates. For instance, the leftmost peak occurs at −815 Hz. It cross-range coordinate is thus,

$$x_1 = \frac{R\lambda}{2v_a} f_D \approx \frac{R_0\lambda}{2v_a} f_D = \frac{(10 \text{ km})(0.03 \text{ m})}{2(100 \text{ m/s})}(-815 \text{ Hz}) = 1220 \text{ m}$$

It is important to note that the above analysis doesn't take into account three important factors which relate to platform motion.

[2]Slow-time is a term used to contrast with fast-time. Fast-time considers return samples within a single PRI. Slow-time considers samples from the same range gate, but taken across PRIs. The Doppler induced phase shifts between successive pulse returns can be analyzed by taking the DFT of the collection of slow-time samples.

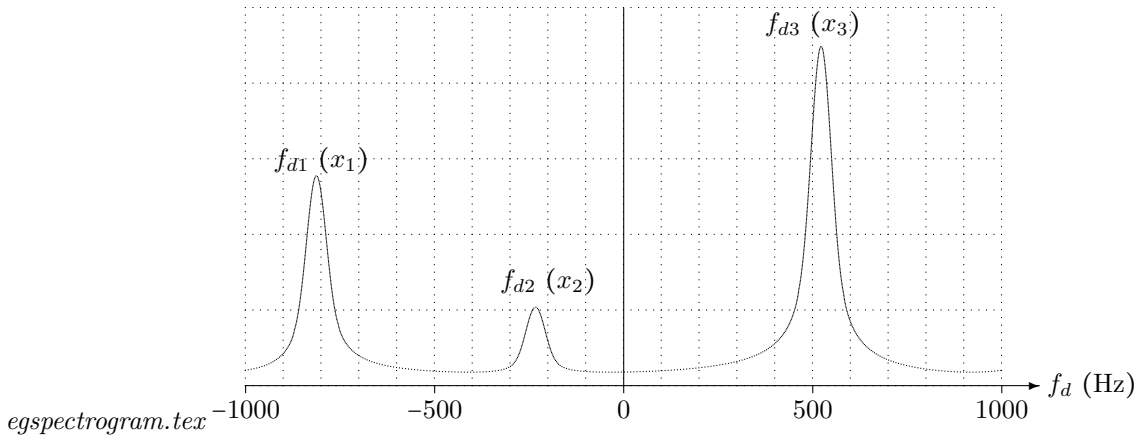

Figure 2.8: Illustration of how a slow-time spectrogram can be used to profile scatterers in cross-range. For MATLAB™/Octave code see appendix A.3.

- As the radar transmits pulses it doesn't remain in the same position. In the case of the example the radar is displaced by 50 meters from when the first pulse is transmitted and the last. This has the effect of adding a quadratic component to the relative phase of successive pulses. This will be dealt with in section 2.4.
- Furthermore, as the platform travels the return for a given scatterer may drift into a different range gate because the slant range from platform to scatterer changes. This effect is known as range migration, and will be dealt with in section **??**.
- The distance used in mapping between Doppler and cross-range was R_0, rather than R. This is because R itself is a function of θ, or equivalently, x, and thus x effectively appears on both sides of the equation, making it more convenient to approximate $R \approx R_0$.

In conclusion, the above computation only yields an approximate value for the cross-range coordinate, and may produce a loss in gain if range migration takes place. SAR processing that limits its observation interval in such a way that none of these effects are significant is called *Unfocused SAR*. Although, processing complexity is greatly reduced, such a SAR cannot achieve the maximum cross-range resolution of $L_a/2$, derived earlier. Unfocused SAR is dealt with in section 2.4.1

2.3.1 Iso-Doppler Contours

Figure 2.9 illustrates the illumination geometry when platform motion is taken into account. The full implication of platform motion on a scatterer's Doppler profile will be investigated later. At this juncture we just wish to derive a relationship between range rate and cross-range that takes it into account.

The platform position is shown at time s. The nadir at time s is given by cross-range coordinate $v_a s$. The relationship governing slant range at time s can be determined easily from the geometry depicted in the figure:

$$R^2 = (x - v_a s)^2 + R_g^2 + h_a^2$$

where R_g is the ground range coordinate of the scatterer.

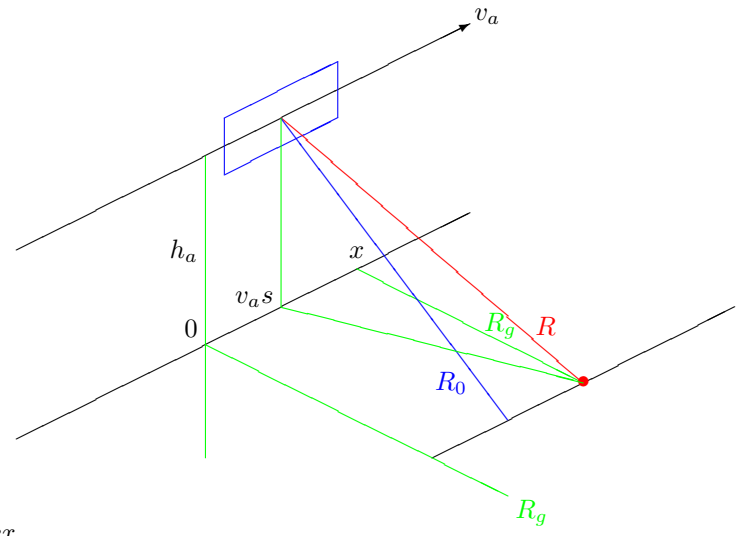

movingplatform.tex

Figure 2.9: Illumination geometry for an off-broadside scatterer with platform motion taken into account.

The range rate may be derived from the above equation:

$$\frac{\mathrm{d}R^2}{\mathrm{d}s} = 2R \cdot \dot{R} = -2(x - v_a s)v_a$$
$$\Rightarrow \dot{R} = \frac{(x - v_a s)v_a}{R}$$

At time zero ($s = 0$) the echo delay, slant range and Doppler are respectively,

$$\tau(0) = \frac{2R(0)}{c} \tag{2.6}$$
$$R^2(0) = x^2 + R_g^2 + h_a^2 \tag{2.7}$$
$$f_d(0) = -\frac{2\dot{R}(0)}{\lambda} = -\frac{\frac{(x-v_a s)v_a}{R}\Big|_{s=0}}{\lambda} = -\frac{2xv_a}{\lambda R(0)} \tag{2.8}$$

Equation 2.7 derives directly from the geometry. Equation 2.8, in which the range rate equation derived above was used, can be solved for $R(0)$

$$R(0) = -\frac{2xv_a}{\lambda f_d(0)}$$

and substituted back into equation 2.7 to yield,

$$\left(-\frac{2xv_a}{\lambda f_d(0)}\right)^2 = x^2 + R_g^2 + h_a^2$$
$$\Rightarrow x^2\left(\left(\frac{2v_a}{\lambda f_d(0)}\right)^2 - 1\right) - R_g^2 = h_a^2$$

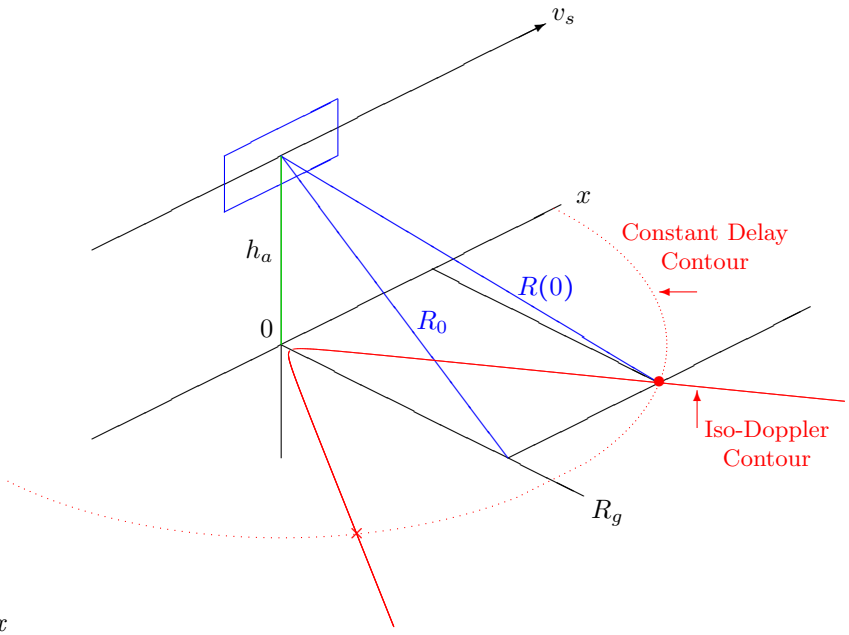

isodopplercontours.tex

Figure 2.10: Iso-Doppler contours.

This equation, when Doppler is treated as a constant, describes a hyperbola in the ground-range/cross-range plane as illustrated in figure 2.10. The above equation can also be expressed as:

$$R_g = \pm\sqrt{x^2\left[\left(\frac{2v_a}{\lambda f_d(0)}\right)^2 - 1\right] - h_a^2}$$

In the figure only the part of the hyperbola corresponding to the + of the squared-root is shown. The minus appears on the other side of the aperture. However, since the aperture only illuminates one side of the plane, it is irrelevant.

It is our goal to demonstrate that a single scatterer can be associated with a specific Doppler, and at this point there is a locus of scatterers (i.e. those that lie on the hyperbola) associated with a single Doppler frequency, $f_D(0)$. We, therefore, need another piece of information, and that is an associated range gate. We note that only two scatterers will intersect the constant delay contour, which is a semi-circle about the origin. The constant delay contour is the locus of scatterers which have the same slant range, $R(0)$, or alternatively, the same echo delay and, are thus, within the same range gate.

The constant delay contour intersects the iso-Doppler contour in two places. The intersection in the positive quadrant corresponds to positive Doppler, as the aircraft travels towards the • scatterer. The intersection in the negative quadrant corresponds to negative Doppler, as the aircraft recedes from the × scatterer.

It has now been demonstrated that in a given range gate there is a unique mapping between Doppler and cross-range. The next step is to demonstrate what is the limit in resolution that can be obtained in cross-range. That is, how close can two scatterers be in cross-range and still be separable?

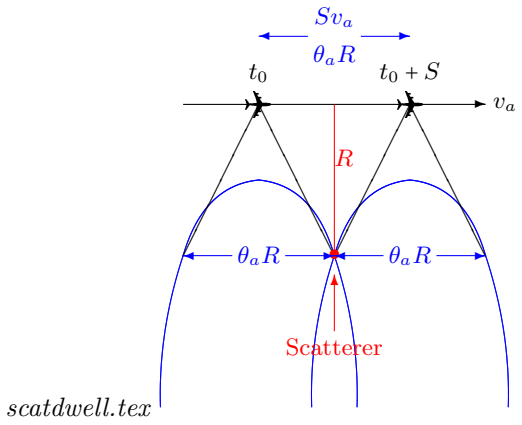

Figure 2.11: Illustration of dwell time on scatterer.

2.3.2 Derivation of cross-range resolution limit

At this junction we are ready to derive the aforementioned limit on range resolution for strip-mode SAR. We begin recalling the relation between cross-range and Doppler (equation 2.4).

$$f_D = \frac{2v_a x}{R\lambda}$$

Thus, the Doppler resolution and cross-range resolution are related by

$$\Delta f_D = \frac{2v_a \Delta x}{R\lambda} \tag{2.9}$$

Now, Doppler resolution depends on the time extent of the observation interval over which the Doppler frequency is being observed, say S.

$$\Delta f_D = \frac{1}{S} \tag{2.10}$$

Clearly, the longer the observation interval, the better Doppler resolution that can be attained. We, therefore, choose the longest possible dwell time on the scatterer, that is, the time extent in which the scatterer is illuminated by the beam footprint. Figure 2.11 illustrates the beam entering and leaving the scatterer. The distance traversed by the platform during this interval is

$$Sv_a = R\theta_a$$

where R is the slant range at closet approach and θ_a is the beamwidth in azimuth. The equality between the left and right sides of the equation is apparent from the figure. Solving for S we have:

$$S = \frac{R\theta_a}{v_a}$$

Substituting back into equation 2.10 we have:

$$\Delta f_D = \frac{1}{S} = \frac{1}{\frac{R\theta_a}{v_a}} = \frac{v_a}{R\theta_a} = \frac{L_a v_a}{R\lambda} \tag{2.11}$$

We utilized equation 2.1 in the last equality.

We can now solve for cross-range resolution using equation 2.9

$$\Delta f_D = \frac{2v_a \Delta x}{R\lambda} \quad \Rightarrow \Delta x = \frac{R\lambda}{2v_a} \cdot \Delta f_D = \frac{R\lambda}{2v_a} \cdot \frac{L_a v_a}{R\lambda} = \frac{L_a}{2} \tag{2.12}$$

This is the result obtained earlier in section 2.2.3.

2.3.3 Practical limit on cross-range resolution

In the preceding section it was shown that cross-range resolution is half the azimuthal antenna length, irrespective of other system parameters. If so, why not arbitrarily reduce the antenna length in order to attain arbitrarily good cross-range resolution?

The first and most obvious answer can be inferred from figure 2.11. Recall, that in deriving the cross-range resolution limit, we chose the longest possible dwell time on the scatterer, which provided the best Doppler resolution, which in turn provided the best attainable cross-range resolution. Maximum dwell time on a scatterer is given by:

$$S = \frac{\theta_a R}{v_a}$$

If the antenna is shortened, the beamwidth is widened (i.e. θ_a is made larger), and thus, S is increased. As $\theta_a \to \infty$, $S \to \infty$. Thus, the amount of dwell time available will limit attainable cross-range resolution.

There is yet another factor that will limit us in terms of achieving infinite cross-range resolution. The narrower the antenna dimensions, the less power density we can achieve. Refer to [5] for a detailed derivation.

2.4 Quadratic Phase and Linear Doppler Spread

Till now we have talked about a scatterer's Doppler as though it was constant throughout the observation interval. However, when choosing a large observation interval, the Doppler inevitably changes throught the collection interval. Figure 2.11 illustrates the aircraft approaching the scatterer at the first half of the dwell interval, and receding in the second half. Thus, a positive Doppler is incurred in the first half, and a negative Doppler in the second half. Furthermore, since the aspect angle with respect to the scatterer changes throughout the flight path, a constantly changing Doppler results. Note, when the aircraft is perpendicularly aligned with the scatterer (i.e. in the center of the dwell interval) the return Doppler is zero, since the aircraft is neither approaching nor receding from the scatterer.

In this section we demonstrate that for the given geometry a quadratic phase is induced in the pulse returns, which in turn produces a linear Doppler spread throughout the observation interval. Two approaches are given on how to contend with the quadratic phase component. The first, *unfocused SAR*, attempts to minimize this component at the expense of cross-range resolution. The second, *focused SAR*, attempts to remove the quadratic phase during processing, and, thus, achieve full cross-range resolution.

2.4.1 Unfocused SAR

Ideally, when processing SAR data we wish to remove the quadratic phase component, retaining only a linear component. This turns out to be computationally expensive, as the quadratic

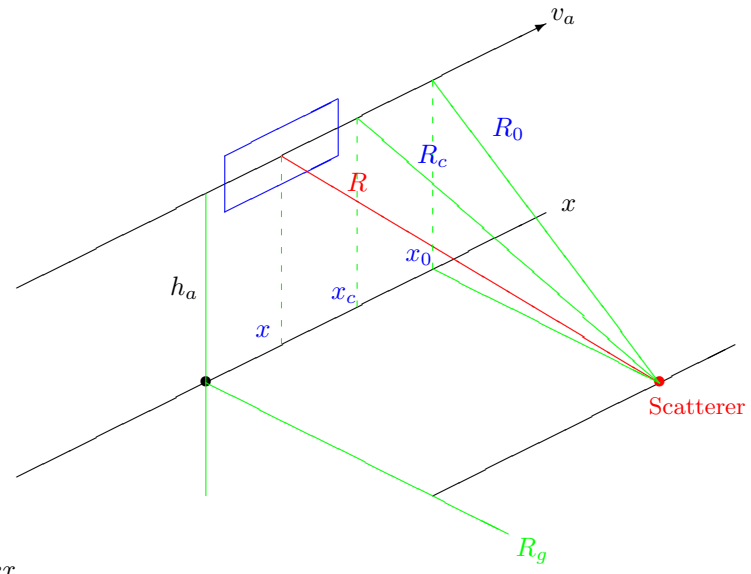

offbroadsidescattaylorexp.tex

Figure 2.12: Geometry used for deriving a relationship between slant range and cross-range.

phase progression is different for each range cell, and for each scatterer within a range cell the quadratic phase progression must be removed separately from the others. The problem is further compounded, if range migration takes place, and the scatterer's returns are spread over a few range cells.

One approach is to limit the observation interval per scatterer to that which the quadratic phase component is negligible, and thus the Doppler can be considered constant throughout the interval. A simple DFT operation can then be used to locate targets in cross-range. This approach is called *unfocused SAR*. However, since the observation interval is relatively short, Doppler resolution will be coarser, and thus, cross-range resolution. Nonetheless, a significant improvement may still be attained over SLAR (which makes no use of Doppler).

Relating between slant range and cross-range

Consider figure 2.12. The antenna is depicted at arbitrary cross-range coordinate, x. The cross-range coordinate of closest approach is denoted x_0. A third coordinate is defined in the center of the observation interval, and denoted x_c. In order to relate between slant range and cross-range we will utilize a Taylor expansion about x_c.

$$R = \sum_{n=0}^{\infty} A_n \frac{(x-x_c)^n}{n!} = A_0 + A_1(x-x_c) + \frac{A_2}{2}(x-x_c)^2 + \ldots, \quad \text{where} \quad A_n = \frac{\mathrm{d}^n}{\mathrm{d}x^n} R(x)\Big|_{x=x_c}$$

The first two Taylor coefficients are computed as follows:

$$\begin{aligned} A_0 &= R(x_c) = R_c \\ A_1 &= \frac{\mathrm{d}}{\mathrm{d}x} R(x)\Big|_{x=x_c} = \frac{\mathrm{d}}{\mathrm{d}x}\sqrt{R_0^2 + (x-x_0)^2}\Big|_{x=x_c} = \frac{1}{2}\left(R_0^2 + (x-x_0)^2\right)^{-\frac{1}{2}} 2(x-x_0)\Big|_{x=x_c} \\ &= \frac{x_c - x_0}{\sqrt{R_0^2 + (x_c-x_0)^2}} = \frac{x_c - x_0}{R_c} \end{aligned}$$

where

- R is slant range from antenna center to scatterer.
- R_c is slant range when antenna projects onto x_c.
- R_0 is slant range when antenna projects onto x_0, that is, slant range of closest approach.

The third Taylor coefficient is computed as follows:

$$\begin{aligned} A_2 &= \frac{\mathrm{d}^2}{\mathrm{d}x^2} R(x)\Big|_{x=x_c} = \frac{\mathrm{d}^2}{\mathrm{d}x^2}\sqrt{R_0^2+(x-x_0)^2}\Big|_{x=x_c} = \frac{\mathrm{d}}{\mathrm{d}x}\frac{1}{2}\left(R_0^2+(x-x_0)^2\right)^{-\frac{1}{2}} 2(x-x_0)\Big|_{x=x_c} \\ &= -\frac{1}{2}\left(R_0^2+(x-x_0)^2\right)^{-\frac{3}{2}} 2(x-x_0)(x-x_0) + \left(R_0^2+(x-x_0)^2\right)^{-\frac{1}{2}}\Big|_{x=x_c} \\ &= \left(R_0^2+(x_c-x_0)^2\right)^{-\frac{3}{2}}(x_c-x_0)^2 + \left(R_0^2+(x_c-x_0)^2\right)^{-\frac{1}{2}} \\ &= R_c^{-3}(x_c-x_0)^2 + R_c^{-1} = \frac{(x_c-x_0)^2+R_c^2}{R_c^3} = \frac{R_0^2}{R_c^3} \end{aligned}$$

Substituting for the coefficients, the Taylor series becomes:

$$R = R_c + \frac{x_c-x_0}{R_c}(x-x_c) + \frac{R_0^2}{2R_c^3}(x-x_c)^2 + \cdots$$

The next step is to compute the phase of the return. Phase is proportional to the two-way distance traveled by the wave:

$$\phi = -\frac{2\pi(2R)}{\lambda} \tag{2.13}$$

The minus sign appears because the signal arrives at a delay rather than in advance.

Note, it is assumed that the two-way travel distance is $2R$. This is not completely accurate, as the travel distance back, will, in general, be different than R, since the platform continues to move as the wave makes its way back to the antenna. However, for platform speeds and distances encountered in airborne SARs it is usually sufficient to approximate the return trip as R.

Substituting for the truncated Taylor representation of R, the phase becomes:

$$\begin{aligned} \phi &\approx -\frac{2\pi\cdot 2\left(R_c + \frac{x_c-x_0}{R_c}(x-x_c) + \frac{R_0^2}{2R_c^3}(x-x_c)^2\right)}{\lambda} \\ &= -\frac{4\pi}{\lambda}\left(R_c + \frac{x_c-x_0}{R_c}(x-x_c) + \frac{R_0^2}{2R_c^3}(x-x_c)^2\right) \end{aligned} \tag{2.14}$$

Higher order terms of the Taylor series expansion have been dropped, since they are usually negligible. Therefore, we are left with a quadratic form for the relative phase of the return.

Relating between Doppler and cross-range

With the phase at hand, it is now possible to obtain an expression for Doppler. However, since the Doppler is quadratic, there will be a Doppler spread, as will soon be demonstrated.

The instantaneous Doppler of the return is defined as the derivative of the phase:

$$f_D = \frac{\mathrm{d}}{\mathrm{d}t}\phi(t) = \left(\frac{\mathrm{d}}{\mathrm{d}x}\phi(t)\right)\left(\frac{\mathrm{d}x}{\mathrm{d}t}\right)$$

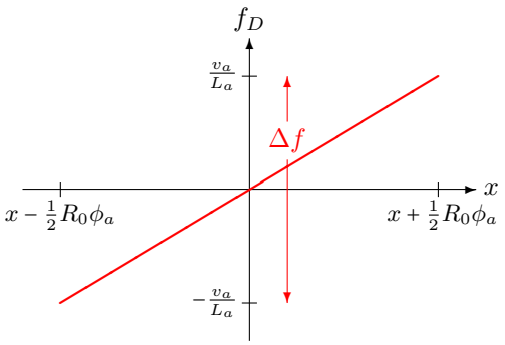

dopvscrossrange.tex

Figure 2.13: Illustration of Doppler spread induced by scatterer.

Note, the invocation of the chain rule. Substituting for ϕ we obtain:

$$\begin{aligned} f_D &= \frac{1}{2\pi}\left(-\frac{4\pi}{\lambda}\right)\frac{\mathrm{d}}{\mathrm{d}x}\left(R_c + \frac{x_c - x_0}{R_c}(x - x_c) + \frac{R_0^2}{2R_c^3}(x - x_c)^2\right)\left(\frac{\mathrm{d}x}{\mathrm{d}t}\right) \\ &= -\frac{2}{\lambda}\left(\frac{x_c - x_0}{R_c} + \frac{R_0^2}{R_c^3}(x - x_c)\right)\left(\frac{\mathrm{d}x}{\mathrm{d}t}\right) \end{aligned}$$

For narrowbeam SAR the approximation $R_o \approx R_c$ can be made. Furthermore, $\frac{\mathrm{d}x}{\mathrm{d}t}$ is simply the aircraft speed, v_a. With this,

$$f_D \approx -\frac{2}{\lambda}\left(\frac{x_c - x_0}{R_0} + \frac{x - x_c}{R_0}\right)v_a = -\frac{2v_a}{\lambda R_0}(x - x_0) \tag{2.15}$$

We see from this expression that Doppler is a linear function of cross-range. At the point of closest approach, the aircraft is neither approaching nor receding from the scatterer, and, therefore, the Doppler is zero:

$$f_D(x_0) = -\frac{2v_a}{\lambda R_0}(x_0 - x_0) = 0$$

Figure 2.13 depicts the linear relationship between cross-range and Doppler. The cross-range axis refers to the cross-range coordinate of the aircraft, whereas x_0 refers to the cross-range coordinate of the scatterer. Δf denotes the Doppler spread of the scatterer within the SAR's field of view.

How were the limits of the Doppler spread shown on the graph attained? To answer this question we must consider the limits on the cross-range where the scatterer is within view of the radar. Recall figure 2.11 showing the scatterer entering and leaving the radar's beam. It is redrawn here as figure 2.14 with emphasis on cross-range. From the figure it is clear that when the aircraft is at coordinate $x_0 - \frac{1}{2}\theta_a R_0$ then the scatterer is just entering the beam, and when at $x_0 + \frac{1}{2}\theta_a R_0$ then the scatterer is just leaving the beam.

We first compute the Doppler as the scatterer enters the beam:

$$f_{D(\min)} = -\left.\frac{2v_a}{\lambda R_0}(x - x_0)\right|_{x_0 - \frac{1}{2}\theta_a R_0} = -\frac{2v_a}{\lambda R_0}(x_0 - \frac{1}{2}\theta_a R_0 - x_0) = -\frac{2v_a}{\lambda R_0}(\frac{1}{2}\frac{\lambda}{L_a}R_0) = -\frac{v_a}{L_a}$$

Likewise, the Doppler as the scatterer leaves the beam is

$$f_{D(\max)} = \frac{v_a}{L_a}$$

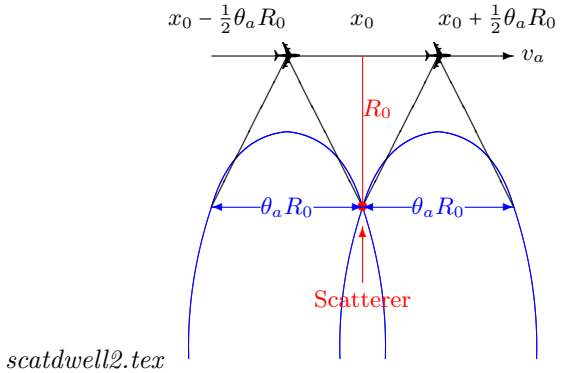

Figure 2.14: Illustration of scatterer entering and leaving the radar beam, and corresponding cross-range coordinate of aircraft and scatterer.

The Doppler spread is thus,

$$\Delta f = f_{D(\max)} - f_{D(\min)} = 2\frac{v_a}{L_a}$$

For the parameters of example 1 and an aircraft flying at 100 m/s, the Doppler spread is:

$$\Delta f = 2\frac{v_a}{L_a} = 2\frac{100 \text{ m/s}}{1 \text{ m}} = 200 \text{ Hz}$$

This means a scatterer will appear spread across 200 Hz on a spectrogram. Recall from equation 2.11 that full Doppler resolution should be

$$\Delta f_D = \frac{L_a v_a}{R_0 \lambda} = \frac{(1 \text{ m})(100 \text{ m/s})}{(5.759 \text{ km})(0.03 \text{ m})} = 0.5788 \text{ Hz}$$

A focused scattered should only have a spread of 0.5788 Hz, and yet because of the quadratic phase component, its Doppler spread is 200 Hz.

In unfocused SAR we wish to keep the processing simple (that is we wish to have the spectrogram be our processing), so we put up with the Doppler spread, except we limit it by limiting the dwell time, as mentioned earlier.

Typically, the deviation of the phase due to the quadratic component (as taken from equation 2.14) is limited to $\pi/4$:

$$\frac{4\pi}{\lambda} \cdot \frac{R_0^2}{2R_c^3}(x - x_c)^2 \leq \pi/4$$

We proceed to express the inequality as follows:

$$\begin{aligned}
&-\sqrt{\frac{\pi}{4}\left(\frac{2R_c^3}{R_o^2}\right)\left(\frac{\lambda}{4\pi}\right)} \leq x - x_c \leq \sqrt{\frac{\pi}{4}\left(\frac{2R_c^3}{R_o^2}\right)\left(\frac{\lambda}{4\pi}\right)} \\
&\Rightarrow -\sqrt{\frac{\lambda R_0}{8}} \leq x - x_c \leq \sqrt{\frac{\lambda R_0}{8}} \\
&\Rightarrow x_c - \sqrt{\frac{\lambda R_0}{8}} \leq x \leq x_c + \sqrt{\frac{\lambda R_0}{8}}
\end{aligned} \tag{2.16}$$

We define X as the range of x's over which the SAR will focus on for a given scatterer, that is, those x's for which the quadratic phase deviation satisfies that above inequality. The assumption is that within X the Doppler doesn't deviate significantly.

$$X = \sqrt{\frac{\lambda R_0}{8}} - \left(-\sqrt{\frac{\lambda R_0}{8}}\right) = \sqrt{\frac{\lambda R_0}{2}}$$

The observation/integration interval of the unfocused SAR is thus,

$$S_{\text{uf}} = \frac{X}{v_a} = \frac{\sqrt{\frac{\lambda R_0}{2}}}{v_a}$$

Note, that variations of the unfocused SAR resolution formula exist in the literature. The differences are in what is deemed acceptable quadratic deviation. For this derivation $\pi/4$ was used.

Recall the relationship between Doppler resolution and cross-range resolution (equation 2.12),

$$\Delta x = \frac{R\lambda}{2v_a} \cdot \Delta f_D$$

Using $\Delta f_D = \frac{1}{S_{\text{uf}}}$ we obtain the cross-range resolution

$$\Delta x = \frac{R\lambda}{2v_a} \cdot \frac{1}{S_{\text{uf}}} = \frac{R\lambda}{2v_a} \cdot \frac{v_a}{\sqrt{\frac{\lambda R_0}{2}}} = \sqrt{\lambda R_0/2}$$

Note that $\Delta x = X$. It should be noted that the resolution is no longer range dependent, as in the limiting case.

Example 2

Compute the resolution obtained in unfocused SAR, using parameters from example 1 and a scatterer at the center of the beam footprint.

Solution:

The scatterer is at a slant range of $R_0 = 5.759$ km (see example 1). The cross-range observation distance satisfying inequality 2.16 is

$$X = \sqrt{\frac{\lambda R_0}{2}} = \sqrt{\frac{(0.03 \text{ m})(5.759 \text{ km})}{2}} = 9.29 \text{ m}$$

This is also the cross-range resolution of the unfocused SAR,

$$\Delta x = X = 9.29 \text{ m}$$

The observation interval on the scatterer is

$$S_{\text{uf}} = \frac{X}{v_a} = \frac{9.29 \text{ m}}{100 \text{ m/s}} = 9.29 \text{ mS}$$

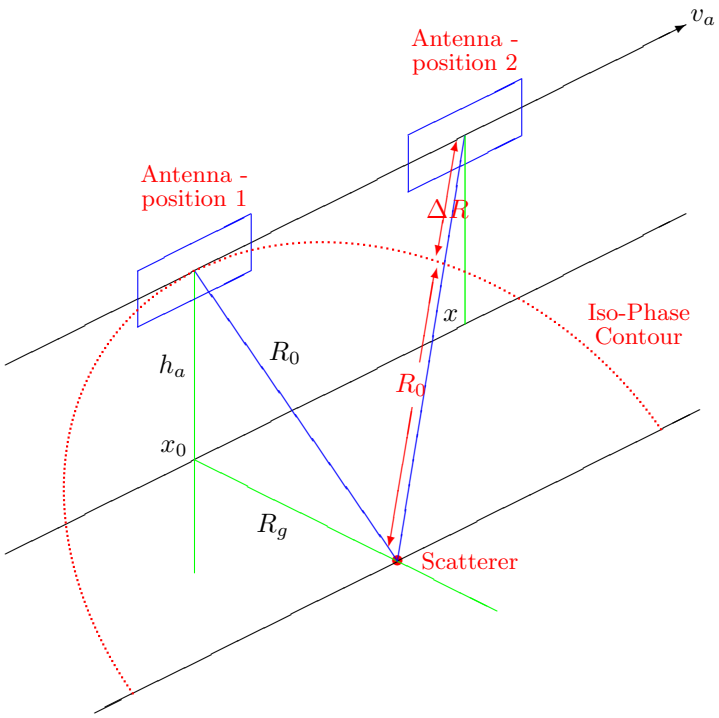

excessphasefig.tex

Figure 2.15: Illustration of excess (quadratic) phase that must be compensated for, in order to remove the linear Doppler spread.

2.4.2 Focused SAR

In focused SAR the excess phase progression that results in a changing Doppler profile as the footprint traverses the target is compensated for and canceled.

Figure 2.15 depicts the antenna at two positions along its flight path.

- At the first position the antenna is broadside to the scatterer, and thus the Doppler is zero. The slant range is the smallest it will be with respect to that scatterer, and denoted R_0.
- In the second position depicted the antenna has moved forward along the flight path such that the scatterer is receding. The slant range is now $R_0 + \Delta R$.

The increased slant range between antenna and scatterer manifests itself as increased phase with respect to broadside. This *relative phase* is given by

$$\Delta\phi = 2(2\pi)\frac{\Delta R}{\lambda} = 4\pi\frac{\Delta R}{\lambda}$$

The factor of "2" accounts for the two-way travel of the radar wave.

Also depicted in the figure is the iso-phase contour, a tilted semi-circle. Any point on the iso-phase contour is at a distance R_0 from the scatterer. If the flight path is coincident with this contour, the Doppler would be zero through out the collection interval.

The objective of a focused SAR algorithm is to compensate for the effect of ΔR, so that there is no Doppler spread for a given scatterer. In order to arrive at the proper compensation

we need to explore the relationship between ΔR and the cross-range coordinate of the antenna platform. From the geometry depicted in the figure the slant range at broadside (position 1) is

$$R_0 = \sqrt{h_a^2 + R_g^2}$$

The slant range at position 2 (which represents an arbitrary non-broadside position) is

$$R(x) = R_0 + \Delta R = \sqrt{h_a^2 + (x - x_0)^2 + R_g^2} = \sqrt{R_0^2 + (x - x_0)^2}$$

Solving for ΔR we have

$$\Delta R = \sqrt{R_0^2 + (x - x_0)^2} - R_0$$

We will now proceed to approximate this expression. At first we normalize ΔR with respect to R_0.

$$\frac{\Delta R}{R_0} = \sqrt{1 + \left(\frac{x - x_0}{R_0}\right)^2} - 1$$

We then use a well known approximation

$$(1 + a)^q \approx 1 + qa, \quad a \ll 1$$

to yield

$$\frac{\Delta R}{R_0} = \sqrt{1 + \underbrace{\left(\frac{x - x_0}{R_0}\right)^2}_{a}} - 1 \approx 1 + \underbrace{\frac{1}{2}}_{q}\left(\frac{x - x_0}{R_0}\right)^2 - 1 = \frac{1}{2}\left(\frac{x - x_0}{R_0}\right)^2$$

In the above approximation, the condition $a \ll 1$ translates into $|x - x_0|^2 \ll R_0^2$, or more simply $|x - x_0| \ll R_0$.

Denormalizing, we obtain

$$\Delta R \approx \frac{(x - x_0)^2}{2R_0} \tag{2.17}$$

The relative phase is thus

$$\Delta\phi = 4\pi\frac{\Delta R}{\lambda} \approx 2\pi\frac{(x - x_0)^2}{\lambda R_0}$$

This result indicates that the phase progression of the incoming radar waves is quadratic with respect to cross-range offset.

Example 3

Consider a SAR whose parameters are given in example 1 and a scatterer at the center of the beam footprint. Additionally, assume:

- Platform velocity of 100 m/s
- PRF 2000 Hz
- 10,000 pulses are collected from the time the SAR is broadside to the scatterer.

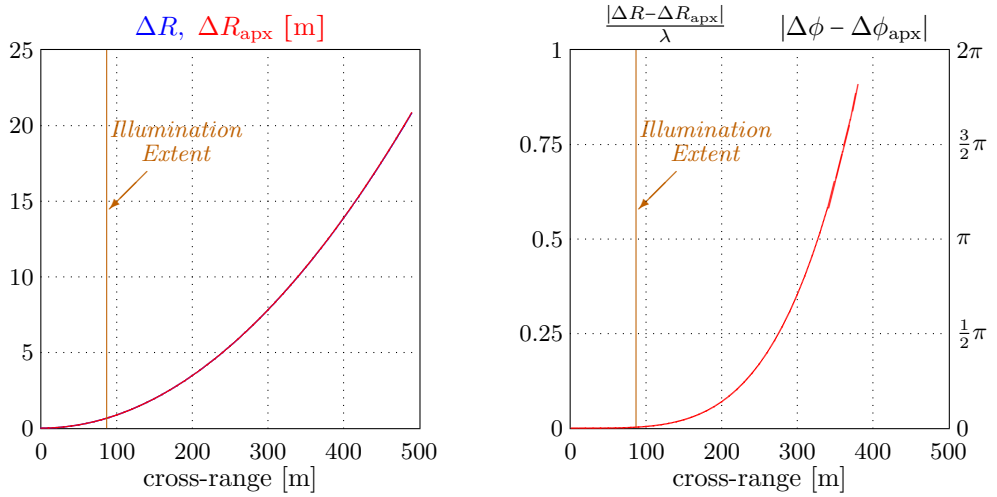

eg3quadphasefig.tex

Figure 2.16: (Right) True ΔR and its approximation. Within the extent plotted the difference is hardly noticeable. (Left) Approximation error of ΔR normalized to λ. This is also the approximation error of relative phase scaled by 2π. The vertical lines labeled "illumination extent" indicate the beamwidth boundaries outside of which the scatterer at x_0 is no longer in view of the antenna.

Plot the true ΔR and its quadratic approximation. Also plot the approximation error $\Delta R - \Delta R_{\text{apx}}$ normalized to the wavelength, which is proportional to the approximation error of the relative phase, $\Delta\phi - \Delta\phi_{\text{apx}}$, by a factor of 2π.

Solution
The PRI is

$$T_r = \frac{1}{F_R} = \frac{1}{2000 \text{ Hz}} = 0.0005 \text{ mS}$$

After 10,000 pulses the radar platform has traversed

$$X = MT_r v_a = (10000)(0.0005 \text{ mS})(100 \text{ m/s}) = 500 \text{ m}$$

The left plot of figure 2.16 shows ΔR and its quadratic approximation as a function of platform (cross-range) position during the 500 m span of data collection that takes place from when the platform is broadside to the scatterer. The right hand plot shows the resulting phase error between the true relative phase and its approximation. For MATLAB™/Octave refer to appendix **??**.

A vertical line on both graphs marks the illumination extent of the beam. That is, at what platform cross-range position within the collection interval is the scatterer no longer within view of the antenna. This would be half the cross-range beamwidth. Using the values computed from example 1 we obtain

$$\frac{1}{2} R_0 \theta_a = \frac{1}{2}(5.308 \text{ km})(0.03 \text{ rad}) = \frac{1}{2}(172.8 \text{ m}) = 86.4 \text{ m}$$

Any data collected by the SAR beyond this cross-range offset is considered not to be of use for processing the scatterer at x_0. It is, however, useful for scatterers beyond x_0.

We will now proceed to interpret the results of the example. The difference between true slant range and its quadratic approximation appears negligible for the cross-range offset range depicted. However, this is not very revealing, as what is important is phase error. This is because the nature of the phase increase is what determines the nature of the Doppler spread. Since phase is modulo 2π it is necessary for the phase error be much less than 2π over the interval of interest, and this is what the right hand graph examines.

The right hand graph is that of range error normalized to wavelength, which is the same as the phase error, scaled by 2π. In order that the approximation should be valid the error should stay well within a cycle of the wavelength, that is

$$|\Delta R - \Delta R_{\text{apx}}| \ll \lambda \quad \Rightarrow \frac{|\Delta R - \Delta R_{\text{apx}}|}{\lambda} \ll 1$$

Equivalently, the phase error must be well under the phase wrap around value of 2π

$$|\Delta\phi - \Delta\phi_{\text{apx}}| \ll 2\pi$$

Clearly this is not the case for the entire data collection interval!

Recall, however, that the given scatterer under examination (i.e. at $x = 0$) is not necessarily illuminated during the entire data collection interval. In fact we rely on the fact that for a reasonably narrow beamwidth, only cross-range offsets that satisfy the approximation condition will have the scatterer within view of the antenna. Referring back to figure 2.15, it is clear that the scatterer has long left the illumination region of the antenna by the time the SAR is at position 2, that is, if a narrow beam aperture is considered. In the example it is clear from the right hand graph that phase error is negligible within the illumination extent of 86.4 m.

As a final note, it is necessary to mention that we only considered data collection from position x_0 and beyond. For full SAR resolution, data collection should include the platform both approaching the scatterer and receding from it. In the example we only showed the latter, although it is clear that the graph would be symmetrical about the origin had we fixed the collection interval to include both.

Removal of quadratic phase term

If the relative phase term is removed from all data collected over the illumination interval $X = \theta_h R_0$ then full SAR resolution can be attained. When the compensated returns are coherently integrated only a target at x_0 has been properly compensated and will be integrated coherently, whereas targets at other distances will not integrate properly since the compensation applied to them is wrong.

Of course, for each cross-range coordinate x_0 we wish to process, we consider the quadratic phase progression associated with that cross-range, and remove it from the data. That is, we treat each cross-range coordinate we are processing as the broadside coordinate, and remove the relative phase from the data based on that. This is depicted in figure 2.17. This is a computationally expensive procedure, since we are removing the phase from the data repeatedly, each time considering a different part of the data as being the phase center.

Although in the figure the assumed scatterer locations being processed are depicted at distance from each other, attaining full SAR resolution means assuming scatterers separated by the resolution limit $L_a/2$, which can be on the order of a meter. A more detailed description of a SAR processor is considered in the next chapter.

At this point we proceed to developed a matched filter interpretation for the optimal SAR processor. The waveform of the uncompensated return (disregarding amplitude) can be expressed as

$$r(x) = \exp\left(j\phi(x)\right)$$

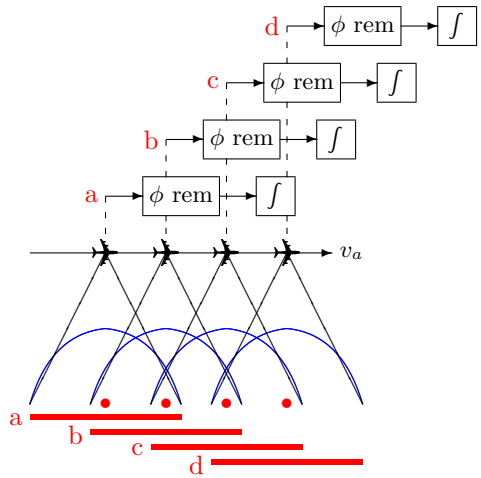

excessphaseremovalfig.tex

Figure 2.17: Illustration of the phase removal procedure in a focused SAR algorithm. Four assumed scatterer locations along cross-range, marked "a", "b", "c" and "d", are to be processed. For each assumed scatterer the quadratic phase removal has to be done on the data, with the phase center of the data corresponding to the location of the airplane at the point it is broadside with the assumed scatterer. If a scatterer is actually there, it will get integrated coherently, whereas the other scatterers will integrate destructively, since the quadratic phase removal was only done correctly for the assumed scatterer. This is repeated for each of the scatterers. That is the quadratic phase is removed anew from the data for the second, third and fourth scatterers. The cross-range illumination extent for each assumed scatterer location is shown at the bottom.

where ϕ was given earlier in equation 2.13 as

$$\phi = -\frac{2\pi(2R(x))}{\lambda}$$

Note, the time component of the return $\exp(j\omega_c t)$ is removed in the heterodyning process, and only the relative phase is left.

Substituting for ϕ and subsequently for R we have

$$\begin{aligned} r(x) &= \exp\left(-j\frac{4\pi R(x)}{\lambda}\right) \\ &= \exp\left(-j\frac{4\pi}{\lambda}\left(R_0 + \Delta R\right)\right) \\ &\approx \exp\left(-j\frac{4\pi}{\lambda}\left(R_0 + \frac{(x-x_0)^2}{2R_0}\right)\right) \end{aligned} \tag{2.18}$$

In the second line R was broken down into the iso-range component (see figure 2.15). In the last line we substituted the quadratic approximation for ΔR as found in equation 2.17.

When processing the return, we assume the presence of a reflecting scatterer broadside to the antenna. We apply the following multiplicative compensation to remove the quadratic phase component of the return

$$\exp\left(j4\pi\lambda\Delta R\right) \approx \exp\left(\frac{j2\pi}{\lambda R_0}(x-x_0)^2\right)$$

The compensation is applied as follows to yield

$$r_c(x) = r(x)\cdot\exp\left(j4\pi\lambda\Delta R\right) = \exp\left(\frac{j4\pi}{\lambda}R_0\right)$$

Note, the compensated return is no longer a function of the cross-range dimension. The compensation makes it as though the radar platform were being flown in a circular path around the scatterer. This circular path was referred to earlier as the "iso-phase contour" shown in figure 2.15. In fact, the compensation has resulted in the broadside scatterer having zero-Doppler, since the Doppler waveform is now a constant, that is, $\exp\left(\frac{j4\pi}{\lambda}R_0\right)$.

The Doppler waveform is the time derivative of the compensated return

$$f_D = \frac{\mathrm{d}}{\mathrm{d}t}\exp\left(\frac{j4\pi}{\lambda}R_0\right) = \frac{\mathrm{d}}{\mathrm{d}x}\exp\left(\frac{j4\pi}{\lambda}R_0\right)\cdot\frac{\mathrm{d}x}{\mathrm{d}t} = 0\cdot v_a = 0$$

Following compensation, *integration* is performed.

$$y(t) = \int_{-\frac{1}{2}X_\theta}^{\frac{1}{2}X_\theta}\exp\left(\frac{j4\pi}{\lambda}R_0\right)\mathrm{d}x = X_\theta\exp\left(\frac{j4\pi}{\lambda}R_0\right)$$

where $X_\theta = \theta_a R_0$ is the cross-range extent of illumination afforded by the aperture on a broadside scatterer for the given slant range. (see figure 2.14).[3] Only energy entering the beam from the broadside scatterer integrates in a completely constructive manner. All off-broadside scatterers integrate in a partially constructive, partially destructive manner, as the compensation for those scatterers leaves them with an uncompensated quadratic phase progression. The precise degree to which energy from off-broadside scatterers becomes mixed with the constructively integrated energy of the broadside scatterer, depends on the *sidelobe characteristics* of the compensation filter.

[3]In practice, the return is a discrete waveform composed of data from multiple PRIs, and the integration is a summation. Details will follow in the next chapter.

Matched filter interpretation of a focused SAR processor

In forming a SAR image we are interested in more than just a single scatterer. To process a swath of scatterers, the procedure is repeated for each location of an assumed scatterer, as was illustrated in figure 2.17. This means a phase removal followed by integration for each scatterer location. This procedure can be formulated as a correlation or matched filter operation, whereby the filter is the compensation factor mentioned earlier

$$g(x) = \exp\left(-j\frac{4\pi}{\lambda}\frac{x^2}{2R_0}\right), \quad |x| \le \frac{1}{2}X_\theta$$

The normalized correlator output is thus

$$y(x') = \frac{1}{X_\theta}\int_{x'-\frac{1}{2}X_\theta}^{x'+\frac{1}{2}X_\theta} r(x)g^*(x-x')\,\mathrm{d}x \tag{2.19}$$

where the superscript asterisk denotes complex conjugation. In the expression, the return waveform, $r(x)$, is being convolved with the conjugate of the matched filter $g(x)$, or alternatively, correlated with a shifted version of $g^*(x)$. Recall, the function $g^*(x)$ is the quadratic phase compensation factor. When considering a scatterer at location x' we wish to make it the broadside scatterer. This is accomplished by shifting the quadratic phase compensation factor to that location, as indicated by $g^*(x-x')$ inside the integral.

The variable x' refers to the location of an assumed scatterer. To process an entire swath of scatterers, x' is stepped up, and the correlation integral computed for each x' in the sequence.

In practice, $r(x)$ is not continuous, but rather consists of discrete samples from gated echos of consecutive pulse transmissions. This will be dealt with in the next chapter.

Ideal response of the matched filter to a point scatterer

At this point we wish to compute the response of the quadratic compensation filter and integrator to a point scatterer. This will give us an *ambiguity function* of sorts.

We place a single point scatterer at cross-range coordinate x_0. Such a scatterer produces the return (see equation 2.18)

$$r_{x_0}(x) = \exp\left(-j\frac{4\pi}{\lambda}\left(R_0 + \frac{(x-x_0)^2}{2R_0}\right)\right), \quad |x-x_0| \le \frac{1}{2}X_\theta$$

The cross-range extent of the return is bounded by $\pm X_\theta$ around the scatterer position due to the beamwidth extent of the aperture. The quadratic compensation for an assumed location x' is

$$g^*_{x'}(x) = \exp\left(j\frac{4\pi}{\lambda}\frac{(x-x')^2}{2R_0}\right) \quad |x-x'| \le \frac{1}{2}X_\theta$$

Here too, the compensation filter is bounded by $\pm X_\theta$ around the assumed scatterer location. This is because we don't wish to expend valuable computational resources for processing scatterer energy that lies in the aperture's sidelobes. Compensating $r_{x_0}(x)$ with $g_{x'}(x)$ and integrating gives us (see equation 2.19)

$$y(x') = \frac{1}{X_\theta}\int_{x_L}^{x_H} r_{x_0}(x)g^*_{x'}(x)\,\mathrm{d}x$$

where a normalization factor X_θ is applied to the correlation integral. The limits of the integral can be divided into three regions:

- Region I: $0 \le x' - x_0 \le X_\theta$
  In this region x' is to the right of x_0, and the overlap is as illustrated in the figure

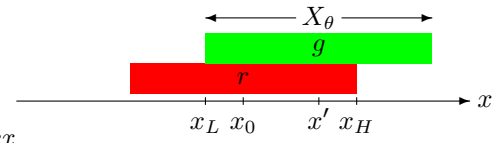

rgoverlap1.tex

  The overlap bounds, which will serve as the limits of integration, are

$$x_L = x' - \frac{1}{2}X_\theta, \quad x_H = x_0 + \frac{1}{2}X_\theta$$

- Region II: $0 \le x_0 - x' \le X_\theta$
  In this region x' is to the left of x_0, and the overlap is as illustrated in the figure.

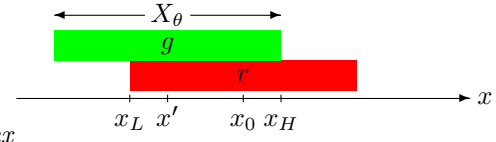

rgoverlap2.tex

  The overlap bounds are

$$x_L = x_0 - \frac{1}{2}X_\theta, \quad x_H = x' + \frac{1}{2}X_\theta$$

- $|x_0 - x'| > X_\theta$
  In this region there is no overlap between $r_{x_0}(x)$ and $g_{x_0}(x)$, in which case $y(x') = 0$.

Substituting for r and g into the correlation integral we obtain

$$\begin{aligned} y(x') &= \frac{1}{X_\theta}\int_{x_L}^{x_H} \exp\left(-j\frac{4\pi}{\lambda}\left(R_0 + \frac{(x-x_0)^2}{2R_0}\right)\right)\exp\left(j\frac{4\pi}{\lambda}\frac{(x-x')^2}{2R_0}\right)\mathrm{d}x \\ &= \frac{1}{X_\theta}\exp\left(-j\frac{4\pi}{\lambda}R_0\right)\int_{x_L}^{x_H}\exp\left(-j\frac{4\pi}{2\lambda R_0}\left[(x-x_0)^2 - (x-x')^2\right]\right)\mathrm{d}x \end{aligned}$$

We'll reduce the argument within the exponential as such:

$$\begin{aligned} (x-x_0)^2 - (x-x')^2 &= x^2 - 2x_0x + x_0^2 - \left(x^2 - 2x'x + x'^2\right) \\ &= 2(x'-x_0)x - (x'^2 - x_0^2) \\ &= 2(x'-x_0)x - (x'+x_0)(x'-x_0) \\ &= 2(x'-x_0)x + (x_0+x')(x'-x_0) \\ &= 2(x'-x_0)\left(x + \frac{x_0+x'}{2}\right) \end{aligned}$$

Thus,

$$\begin{aligned} y(x') &= \frac{1}{X_\theta}\exp\left(-j\frac{4\pi}{\lambda}R_0\right)\int_{x_L}^{x_H}\exp\left(-j\frac{4\pi}{2\lambda R_0}2(x'-x_0)\left(x-\frac{x_0+x'}{2}\right)\right)\mathrm{d}x \\ &= \frac{1}{X_\theta}\exp\left(-j\frac{4\pi}{\lambda}R_0\right)\frac{\exp\left(-j\frac{4\pi}{\lambda R_0}(x'-x_0)\left(x-\frac{x_0+x'}{2}\right)\right)}{-j\frac{4\pi}{\lambda R_0}(x'-x_0)}\Bigg|_{x_L}^{x_H} \\ &= \frac{1}{X_\theta}\exp\left(-j\frac{4\pi}{\lambda}R_0\right)\cdot\exp\left(j\frac{4\pi}{\lambda R_0}(x'-x_0)\cdot\frac{x_0+x'}{2}\right)\cdot\frac{\exp\left(-j\frac{4\pi}{\lambda R_0}(x'-x_0)x\right)}{-j\frac{4\pi}{\lambda R_0}(x'-x_0)}\Bigg|_{x_L}^{x_H} \\ &= \frac{1}{X_\theta}\exp\left(-j\frac{4\pi}{\lambda}R_0\right)\cdot\exp\left(j\frac{4\pi}{\lambda R_0}(x'-x_0)\cdot\frac{x_0+x'}{2}\right) \\ &\quad\cdot\frac{\exp\left(-j\frac{4\pi}{\lambda R_0}(x'-x_0)x_H\right)-\exp\left(-j\frac{4\pi}{\lambda R_0}(x'-x_0)x_L\right)}{-j\frac{4\pi}{\lambda R_0}(x'-x_0)} \end{aligned}$$

We substitute for x_H and x_L applicable to region I.

$$\begin{aligned} y(x') &= \frac{1}{X_\theta}\exp\left(-j\frac{4\pi}{\lambda}R_0\right)\cdot\exp\left(j\frac{4\pi}{\lambda R_0}(x'-x_0)\cdot\frac{x_0+x'}{2}\right) \\ &\quad\cdot\frac{\exp\left(-j\frac{4\pi}{\lambda R_0}(x'-x_0)(x_0+\frac{1}{2}X_\theta)\right)-\exp\left(-j\frac{4\pi}{\lambda R_0}(x'-x_0)(x'-\frac{1}{2}X_\theta)\right)}{-j\frac{4\pi}{\lambda R_0}(x'-x_0)} \end{aligned}$$

Use

$$e^a - e^b = e^{\frac{a+b}{2}}\cdot\left(e^{\frac{a-b}{2}}-e^{\frac{b-a}{2}}\right) = e^{\frac{a+b}{2}}\cdot\left(e^{\frac{a-b}{2}}-e^{-\frac{a-b}{2}}\right)$$

to express the correlator output as

$$\begin{aligned} y(x') &= \frac{1}{X_\theta}\exp\left(-j\frac{4\pi}{\lambda}R_0\right)\cdot\exp\left(j\frac{4\pi}{\lambda R_0}(x'-x_0)\frac{x_0+x'}{2}\right)\cdot\exp\left(-j\frac{4\pi}{\lambda R_0}(x'-x_0)\cdot\frac{x_0+x'}{2}\right) \\ &\quad\cdot\frac{\exp\left(-j\frac{2\pi}{\lambda R_0}(x'-x_0)(x_0-x'+X_\theta)\right)-\exp\left(j\frac{2\pi}{\lambda R_0}(x'-x_0)(x_0-x'+X_\theta)\right)}{-j\frac{4\pi}{\lambda R_0}(x'-x_0)} \end{aligned}$$

Note that the second and third exponential factors cancel each other out. Use the identity $\sin(\phi) = \frac{e^{j\phi}-e^{-j\phi}}{j2}$ to express the correlator output as follows

$$y(x') = \frac{1}{X_\theta}\exp\left(-j\frac{4\pi}{\lambda}R_0\right)\cdot\frac{\sin\left(\frac{2\pi}{\lambda R_0}(x'-x_0)(x_0-x'+X_\theta)\right)}{\frac{2\pi}{\lambda R_0}(x'-x_0)}$$

The right-most parenthesis inside the sin can be expressed as

$$x_0 - x' + X_\theta = X_\theta - (x'-x_0) = X_\theta - |x'-x_0|$$

The last equality hold in region I, where $x' > x_0$. Having the absolute value will be helpful further on when we establish a single expression applicable to both regions I and II. Thus for region I,

$$y(x') = \frac{1}{X_\theta}\exp\left(-j\frac{4\pi}{\lambda}R_0\right)\cdot\frac{\sin\left(\frac{2\pi}{\lambda R_0}(x'-x_0)(X_\theta-|x'-x_0|)\right)}{\frac{2\pi}{\lambda R_0}(x'-x_0)} \tag{2.20}$$

We will apply the same procedure to obtain an expression applicable to region II. We substitute the appropriate x_H and x_L for that region, and apply the same identities as before.

$$\begin{aligned} y(x') &= \frac{1}{X_\theta}\exp\left(-j\frac{4\pi}{\lambda}R_0\right)\cdot\exp\left(j\frac{4\pi}{\lambda R_0}(x'-x_0)\cdot\frac{x_0+x'}{2}\right) \\ &\quad\cdot\frac{\exp\left(-j\frac{2\pi}{\lambda R_0}(x'-x_0)(x'+\frac{1}{2}X_\theta)\right)-\exp\left(-j\frac{2\pi}{\lambda R_0}(x'-x_0)(x_0-\frac{1}{2}X_\theta)\right)}{-j\frac{4\pi}{\lambda R_0}(x'-x_0)} \\ &= \frac{1}{X_\theta}\exp\left(-j\frac{4\pi}{\lambda}R_0\right)\cdot\exp\left(j\frac{4\pi}{\lambda R_0}(x'-x_0)\frac{x_0+x'}{2}\right)\cdot\exp\left(-j\frac{4\pi}{\lambda R_0}(x'-x_0)\cdot\frac{x_0+x'}{2}\right) \\ &\quad\cdot\frac{\exp\left(-j\frac{2\pi}{\lambda R_0}(x'-x_0)(x'-x_0+X_\theta)\right)-\exp\left(j\frac{2\pi}{\lambda R_0}(x'-x_0)(x'-x_0+X_\theta)\right)}{-j\frac{4\pi}{\lambda R_0}(x'-x_0)} \\ &= \frac{1}{X_\theta}\exp\left(-j\frac{4\pi}{\lambda}R_0\right)\cdot\frac{\sin\left(\frac{2\pi}{\lambda R_0}(x'-x_0)(x'-x_0+X_\theta)\right)}{\frac{2\pi}{\lambda R_0}(x'-x_0)} \end{aligned}$$

The right most parenthesis inside the sin can be expressed as

$$x'-x_0+X_\theta = X_\theta-(x_0-x') = X_\theta-|x'-x_0| = X_\theta-|x_0-x'|$$

Thus,

$$y(x') = \frac{1}{X_\theta}\exp\left(-j\frac{4\pi}{\lambda}R_0\right)\cdot\frac{\sin\left(\frac{2\pi}{\lambda R_0}(x'-x_0)(X_\theta-|x'-x_0|)\right)}{\frac{2\pi}{\lambda R_0}(x'-x_0)} \tag{2.21}$$

Observe that equations 2.20 and 2.21 are identical. Therefore, the correlator output for both regions I and II can be expressed by the bounded expression

$$y(x') = \frac{1}{X_\theta}\exp\left(-j\frac{4\pi}{\lambda}R_0\right)\cdot\frac{\sin\left(\frac{2\pi}{\lambda R_0}(x'-x_0)(X_\theta-|x'-x_0|)\right)}{\frac{2\pi}{\lambda R_0}(x'-x_0)}, \quad |x'-x_0|\le X_\theta \tag{2.22}$$

With slight manipulation, equation 2.22 can be expressed in terms of the sinc[4] function.

$$\begin{aligned} y(x') &= \frac{1}{X_\theta}\exp\left(-j\frac{4\pi}{\lambda}R_0\right)\cdot\frac{\sin\left(\frac{2\pi}{\lambda R_0}(x'-x_0)(X_\theta-|x'-x_0|)\right)}{\frac{2\pi}{\lambda R_0}(x'-x_0)\,(X_\theta-|x'-x_0|)}(X_\theta-|x'-x_0|) \\ &= \exp\left(-j\frac{4\pi}{\lambda}R_0\right)\cdot\mathrm{sinc}\left(\frac{2\pi}{\lambda R_0}(x'-x_0)(X_\theta-|x'-x_0|)\right)\frac{X_\theta-|x'-x_0|}{X_\theta} \end{aligned} \tag{2.23}$$

The magnitude of the correlated output is

$$|y(x')| = \left|\mathrm{sinc}\left(\frac{2\pi}{\lambda R_0}(x'-x_0)(X_\theta-|x'-x_0|)\right)\right|\cdot\frac{X_\theta-|x'-x_0|}{X_\theta} \tag{2.24}$$

Example 4

[4]The sinc(x) function is defined here as $\frac{\sin(x)}{x}$. Another commonly used definition, including that which is used in MATLAB™/Octave, is $\frac{\sin(\pi x)}{\pi x}$.

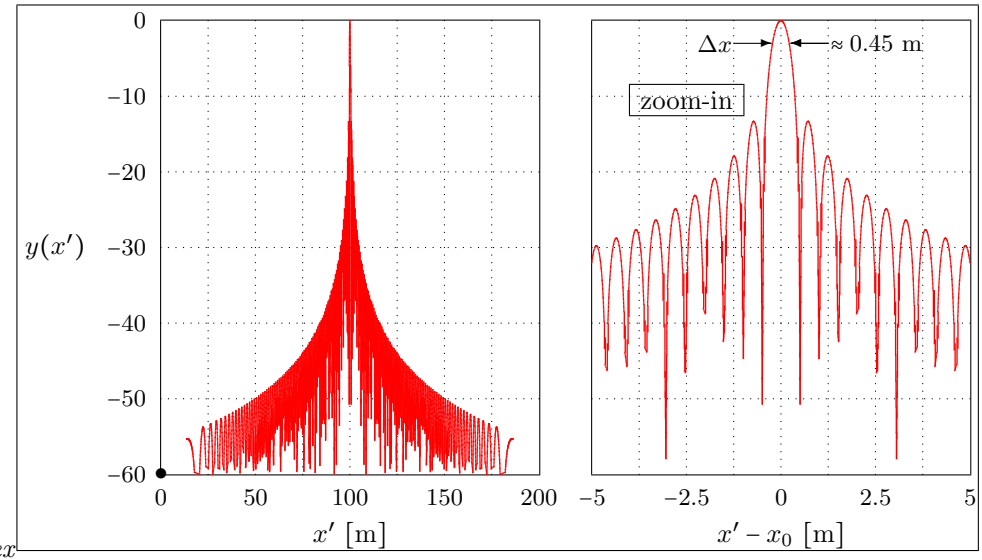

corroutputplotfig.tex

Figure 2.18: A plot of the normalized correlator output (left). A zoomed in section ±5 m about the scatterer boresight.

Compute and plot the magnitude of the normalized correlation output for a scatterer at x_0 = 100 m. Assume the parameters of example 1 and example 3.

Solution
From previous examples λ = 0.03 m, θ_a = 0.03 rad and R_0 = 5758.8 m. The illumination extent for the given slant range is

$$X_\theta = \theta_a R_0 = (0.03 \text{ rad})(5758.8 \text{ m}) = 172.8 \text{ m}$$

The magnitude of the correlator output is thus

$$\begin{aligned} |y(x')| &= \left|\text{sinc}\left(\frac{2\pi}{(0.03 \text{ m})(5758.8 \text{ m})}(x' - 100 \text{ m})(172.8 - |x' - 100 \text{ m}|)\right)\right| \cdot \frac{172.8 \text{ m} - |x' - 100 \text{ m}|}{172.8 \text{ m}} \\ &= \left|\text{sinc}\left(2\pi \frac{(x' - 100 \text{ m})(172.8 - |x' - 100 \text{ m}|)}{172.8 \text{ m}^2}\right)\right| \cdot \frac{172.8 \text{ m} - |x' - 100 \text{ m}|}{172.8 \text{ m}}, \quad |x' - 100| \le 86.4 \text{ m} \end{aligned}$$

A plot of $|y(x')|$ is shown in figure 2.18. From the zoomed-in section (shown on the right) the 3 dB resolution appears to be about 0.45 m, which is in proximity with the expected value of 0.5 m.

Chapter 3

SAR Processing

3.1 The Optimal SAR Processor when no Range Migration Occurs

Fill in theory...

Example 3

Consider a SAR based on example 1. If full SAR resolution is to be attained, how many scatterers are to be processed in a 1 km cross-range swath? Describe the computational load involved in processing, just this one range gate across the enter swath if a PRF of 200 Hz is utilized. Assume the cross-range strip at ground range corresponding to the center of the beam footprint.

If the radar is to attain a slant range resolution equal to the cross-range resolution, what is the pulse width that must be transmitted. What is the total processing load required to process a 1 km range swath?

Solution

The ground range at the center of the beam footprint was computed in example 1 to be 5.671 km. The illumination extent at that ground range is 172.7 m. The cross-range resolution limit is range-independent and stands at 0.5 m.

This means the scatterers marked "abc..." in figure 2.17 are separated by half a meter. There are 2000 assumed scatterers in the entire cross-range swath of 1 km at the range gate of interest.

Just to provide an idea of the processing load consider that for each of the 2000 assumed scatterer locations, a quadratic phase removal has to be performed on pulse transmissions that fall within 172.7 m. Between two pulse transmissions the radar platform traverses

$$\frac{v_a}{F_r} = \frac{100 \text{ m/s}}{200 \text{ Hz}} = 0.5 \text{ m}$$

Therefore, there are 173 pulse samples that fall within the illumination extent of each assumed scatterer location. Those must have the quadratic phase removed from them and integrated. This procedure is repeated for the 2000 scatterers being processed. Consider a quadratic phase removal from a single sample as requiring a single complex operation, and subsequent integration as also requiring a single complex operation per sample. The total complex operations required for the range gate of interest, are thus,

$$2000 \times (2)173 = 692 \times 10^3$$

To attain a slant range resolution equal to the cross-range resolution, which is 0.5 m, the compressed pulse width must be:

$$\tau = \frac{2\Delta R}{c} = \frac{2(0.5 \text{ m}}{3 \times 10^8 \text{ m/s}} = 3.3 \ \mu\text{S}$$

In a 1 km slant range swath, there are $\frac{1 \text{ km}}{0.5 \text{ m}} = 2000$ range bins. Assume that for each cross-range swath the number of complex operations is the same for all range bins. This, of course, is only approximately true, as the number of pulse samples that must have a phase removal and subsequent integration changes from range bin to range bin, since the illumination extent is a function of distance (172.7 m is only at the center of the beam footprint).

Given that, the total computational load is $2000(692 \times 10^3) = 1.384 \times 10^9$

Complete example...

Continue from here...

Appendix A

Simulation Code

This appendix contains the MATLAB™/Octave routines used to calculate results, perform simulations and generate graphs throughout the document.

A.1 Common

The following code defines some physical constants and conversion factors. It is accessed by many of the routines that follow.

```
% ********** Physical constants and conversion factors **********
c = 3e8; % [m/sec] % speed of light in vaccuum
d2r = pi/180; % multiply with d2r to convert degrees to radians
r2d = 180/pi; % multiply with r2d to convert radians to degrees
um2cm = 1e-4; % cm to um
ft2m = 12*2.54/100; % foot to meter
```

The following routine is used to convert some 3D graphs on a rotated/sheared plane.

```
function xy = rotshear(thetax,thetay,xyz)
% function xy = rotshear(thetax,thetay,xyz)
%   Rotate and shear coordinate
%   Provide:
%     thetay = angle of y-axis with respect to true x
%     thetax = angle of x-axis with respect to true y
%     xyz = true 3-D coordinate
%   Returns
%     xy = 2-D
%   Written by Yaron Seliktar

xy = [cos(thetax) cos(thetay) 0; -sin(thetax) sin(thetay) 1]*xyz;
```

A.2 Code for example 1

The following code was used to generate the results for example 1.

```
% Example 1: basic SAR simulation
% Written by Yaron Seliktar
clear
defs

% define and set flag to let examples files that depend on this one know it
% has been run
eg1flag=1;

% System params
fc = 10e9; % [Hz] carrier frequency
La = 1; % [m] aperture length (along-track)
Wa = 1; % [m] aperture width (height)
tau = 10e-9; % [S] pulse width after pulse compression

% Positional params
ha = 1e3; % [m] platform height above nadir
vs = 100; % [m/s] platform speed (denoted vs in curlander)

% Computations
lambda = c/fc; % [m] wavelength
psi = 10*d2r; % [rad] angle of incidence / grazing angle / depression angle
gamma = pi/2-psi; % [rad] look angle
thetaa = lambda/La % [rad] horizontal beamwidth
thetae = lambda/Wa % [rad] vertical beamwidth
% swath
Rs = ha/cos(gamma) % [m] range to center of footprint
Rsmin = ha/cos(gamma-thetae/2) % [m] slant range to near end of footprint
Rsmax = ha/cos(gamma+thetae/2) % [m] slant range to far end of footprint
Rg = ha*tan(gamma) % [m] ground range at center of footprint
Rgmin = ha*tan(gamma-thetae/2) % [m] ground range to near end of footprint
Rgmax = ha*tan(gamma+thetae/2) % [m] ground range to far end of footprint
Ws = Rs*thetae % [m] slant swath width
Wg = Ws/cos(psi) % [m] ground swath width
% resolution
delRs = c*tau/2 % [m] range (cell) resolution
delRg = delRs*sec(psi); % ground resolution at footprint center
delRgmin = delRs*sec(psi-thetae/2); % ground resolution at near end of footpri
delRgmax = delRs*sec(psi+thetae/2); % ground resolution at far end of footprin
Ls = Rs*thetaa % [m] synthetic aperture length
% SLAR resolution
delX = thetaa*Rs; % [m] SLAR resolution at footprint center
% theoretical resolution
delXs = 0.5*La; % [m] theoretical limit on cross-range resolution

printf('Provided:\n');
printf('  platform height (ha) = %0.3f km\n',ha);
printf('  carrier freq (fc) = %0.3f GHz\n',fc/1e9);
printf('  antenna width (Wa) = %0.2f m\n',Wa);
```

```
printf('␣␣antenna␣length␣(La)␣=␣%0.2f␣m\n',La);
printf('␣␣depression␣angle␣(psi)␣=␣%0.2f␣deg␣=␣%0.4f␣rad\n',psi*r2d,psi);
printf('␣␣pulse␣duration␣post␣compression␣(tau)␣=␣%0.2f␣ S \n',tau*1e6);
printf('Computed:\n');
printf('␣␣look␣angle␣(  )␣=␣%0.2f␣deg␣=␣%0.4f␣rad\n',gamma*r2d,gamma);
printf('␣␣wavelength␣(  )␣=␣%0.4f␣m\n',lambda);
printf('␣␣azimuth␣beamwidth␣(  a )␣=␣%0.2f␣deg␣=␣%0.4f␣rad\n',thetaa*r2d,thetaa);
printf('␣␣elevation␣beamwidth␣(  a )␣=␣%0.2f␣deg␣=␣%0.4f␣rad\n',thetae*r2d,thetae);
printf('␣␣Rs␣=␣%0.3f␣km\n',Rs/1e3);
printf('␣␣Rsmin␣=␣%0.3f␣km\n',Rsmin/1e3);
printf('␣␣Rsmax␣=␣%0.3f␣km\n',Rsmax/1e3);
printf('␣␣Rg␣=␣%0.3f␣km\n',Rg/1e3);
printf('␣␣Rgmin␣=␣%0.3f␣km\n',Rgmin/1e3);
printf('␣␣Rgmax␣=␣%0.3f␣km\n',Rgmax/1e3);
printf('␣␣delRs␣=␣%0.3f␣m\n',delRs);
printf('␣␣delRg␣=␣%0.3f␣m\n',delRg);
printf('␣␣delRgmin␣=␣%0.3f␣m\n',delRgmin);
printf('␣␣delRgmax␣=␣%0.3f␣m\n',delRgmax);
printf('␣␣delX␣(SLAR)␣=␣%0.3f␣m\n',delX);
printf('␣␣delXs␣(SAR)␣=␣%0.3f␣m\n',delXs);
```

A.3 Code for figure 2.8

The following simulation code was used to generate figure 2.8.

```
% egspectrogram.m - computes a sample spectrogram of raw PRI samples
% to illustrate how Doppler and cross-range are related.
% Written by Yaron Seliktar
clear

physconst
conversions;

% params
fc = 10e9; % [Hz] carrier frequency
lambda = c/fc; % [m] wavelength
vst = 100; % [m/s] aircraft speeds
R0 = 10000; % [m] nominal (at boresight) slant range
M = 1000; % [] number of pulses collected in observation interval
Fr = 2e3; % [Hz] pulse retition rate = maximum unambiguous Doppler

% define scatterer points in cross range.
phidel = [-0.5:0.01:0.5];
Adel = exp(-phidel.^2*20);

phisdeg = [-7+phidel -2+phidel 4.5+phidel]; % [deg] scatterer angles
Ns = length(phisdeg); % [] No. scatterers
As = kron([3 1 5],Adel); % [] relative amplitude of scatterers
```

```
% convert to Doppler
fd = 2*vst*sin(phisdeg*d2r)/lambda;
% normalized Doppler
fdn = fd/Fr;

r = zeros(1,M);
mrang = [0:M-1];
for s=1:Ns
  r = r + As(s)*exp(j*2*pi*mrang*fdn(s));
end

% Spectrogram of return samples for given range gate
fdrang = Fr*((0:M-1)-M/2)/M; % Doppler axis
Frr = fft(r);
Frrabs = abs(fftshift(Frr));

% display results
plot(fdrang,Frrabs);
```

A.4 Code for figure 2.10

The following code was used to help generate figure 2.10.

```
% Example 2: Iso-Doppler contours
% Written by Yaron Seliktar
if exist('eg1flag','var')
  va = 100; % [m/s] aircraft speeds
  M = 1000; % [] number of pulses collected in observation interval
  Fr = 2e3; % [Hz] pulse retition rate = maximum unambiguous Doppler
  fd0 = [200]; % [Hz] Doppler of scatterer at time zero for iso-Doppler contou
  % Cross-range coordinates for which to compute contour
  xp = [0:1e3]; % [m] positive cross-range coord's
  xn = -xp(end:-1:1); % [m] negative cross-range coord's
  Rgscale = 0.05; % [] scale factor for Rg axis

  printf('Provided:\n');
  printf('  platform speed relative to Earth (va) = %0.3f m/s\n',va);
  printf('  number of pulses (M) = %d\n',M);
  printf('  PRF (Fr) = %0.1f Hz\n',Fr);
  printf('  iso-Doppler contour (fd0) = %0.1f Hz\n',fd0);

  % Iso-Doppler computations
  k1 = 2*va/lambda;
  % compute for positive cross-range coord's
  idx1 = find(xp.^2*(k1^2/fd0^2-1)<ha^2);
  Rgp = sqrt(xp.^2*k1^2/fd0.^2-ha^2);
  Rgp(idx1) = nan;
  idx2 = find(!isnan(Rgp));
  xp1 = xp(idx2);
```

```
Rgp1 = Rgp(idx2);
% -> compute Rg scaling factor
Rgscale = xp(end)/Rgp(end); % scales things so that x,y axes are of eq. length
Rgscale = 0.02; % use a scale that makes the plot "look good"

% -> compute for negative cross-range coord's
xn1 = -xp1;
Rgn1 = -Rgp1;

% Iso-delay computations
% -> select delay for which to compute iso-delay contour
Rs = 807; % [m] range of scatterer
%taus = 2*c/Rs; % [m] delay of scatterer at first pulse
% x^2 + Rg^2 = Rs^2
xx = [0:10:Rs];
Rgiso = sqrt(Rs^2 - xx.^2);

% Plots
figure(1)
plot(xn1/1e3,Rgn1/1e3); hold on
plot(xn1/1e3,-Rgn1/1e3);
plot(xp1/1e3,Rgp1/1e3);
plot(xp1/1e3,-Rgp1/1e3);
plot(xx/1e3,-Rgiso/1e3);
hold off
xlabel('cross-range␣[km]');
ylabel('Rg␣[km]');
grid

% -> plot iso-Doppler on a rotated and sheared plane
theta1 = 0.46365;
aa = rotshear(theta1,theta1,[xp1; Rgn1*Rgscale; zeros(1,length(xp1))]);
bb = rotshear(theta1,theta1,[xp1; -Rgn1*Rgscale; zeros(1,length(xp1))]);
cc = rotshear(theta1,theta1,[xn1; Rgn1*Rgscale; zeros(1,length(xn1))]);
dd = rotshear(theta1,theta1,[xn1; -Rgn1*Rgscale; zeros(1,length(xn1))]);
% --> x-axis
xx1 = [0 max(xp1)];
% --> y-axis
yy1 = [0 max(Rgp1*Rgscale)];
% --> z-axis
zz1 = [0 ha];
ee = rotshear(theta1,theta1,[xx1; 0 0; 0 0]);
ff = rotshear(theta1,theta1,[0 0; yy1; 0 0]);
gg = rotshear(theta1,theta1,[0 0; 0 0; zz1]);
figure(2)
% contours
plot(aa(1,:),aa(2,:)); hold on
plot(bb(1,:),bb(2,:));
plot(cc(1,:),cc(2,:));
```

```
  plot(dd(1,:),dd(2,:));
  % axes
  plot(ee(1,:),ee(2,:),'k');
  plot(ff(1,:),ff(2,:),'k');
  plot(gg(1,:),gg(2,:),'k');

  % -> plot iso-delay on a rotated and sheared plane
  hh = rotshear(theta1,theta1,[xx; Rgiso; zeros(1,length(xx))]);
  ii = rotshear(theta1,theta1,[xx(end:-1:1); -Rgiso(end:-1:1); zeros(1,length(
  plot([hh(1,:) ii(1,:)],[hh(2,:) ii(2,:)]);
  hold off
else
  printf("Must run eg1sar first.\n")
end
```

A.5 Code for example 2

The following code was used to generate the results for example 2.

```
% Example 2: unfocused SAR resolution
% Written by Yaron Seliktar
if exist('eg1flag','var')
  va = 100; % [m/s] aircraft speeds
  eg2flag=1;

  R0 = Rs; % [m] range to center of footprint, we'll make it range to scattere
  X = sqrt(R0*lambda/2); % [m] range over which unfocused SAR integrates
  Sufoc = X/va; % [sec] unfocused interval of observation/integration
  delxunfoc = R0*lambda/(2*va)/Sufoc; % [m] cross-range resolution

  printf('Provided:\n');
  printf('␣␣R0␣=␣%0.3f␣km␣(from␣example␣1)\n',Rs/1e3);
  printf('Computed:\n');
  printf('␣␣X␣=␣%0.3f␣m\n',X);
  printf('␣␣Sufoc␣=␣%0.2f␣mS\n',Sufoc*1e3);
  printf('␣␣delxunfoc␣=␣%0.3f␣m\n',delxunfoc);
else
  printf("Must run eg1sar first.\n")
end
```

A.6 Code for example 3

The following code was used to generate the results for example 3.

```
% Illustrate deviation of quadratic phase from true relative phase
% Written by Yaron Seliktar
if exist('eg1flag','var')
  % obtained from eg1
```

```
x0 = 0; % [m] cross-range coordinate of scatterer
R0 = Rs; % [m] range to center of footprint, we'll make it range to scatterer
% newly defined parameters
va = 100; % [m/s] aircraft speeds
M = 10000; % number of pulses collected in observation interval
Fr = 2e3; % [Hz] pulse retition rate = maximum unambiguous Doppler
% computed
Tr = 1/Fr; % [S] PRI
X = M*Tr*va; % [m] distance covered by platform during data collection

% Delta R
m = [0:M-1]; % pulse indecies
x = m*Tr*va;
delRappx = (x-x0).^2/(2*R0);
Rx = sqrt(ha^2+(x-x0).^2+Rg.^2);
delR = Rx - R0;

% relative phase
delphi = 4*pi*delR/lambda;
delphiappx = 4*pi*delRappx/lambda;

printf('Provided:\n');
printf('  platform height (ha) = %0.3f km\n',ha);
printf('  platform speed relative to Earth (va) = %0.3f m/s\n',va);
printf('  number of pulses (M) = %d\n',M);
printf('  PRF (Fr) = %0.1f Hz\n',Fr);
printf('  R0 = %0.3f km\n',R0/1e3);
printf('  Cross-range beamwidth = %0.1f m\n',delX);
printf('Computed:\n');
printf('  Distance traversed by aircraft during collection = %0.3f km\n',X/1e3);

figure(1);
subplot(3,1,1);
plot(x,delR,'b',x,delRappx,'g');
title('delR and quadratic apprx to delR');
ylabel('delR (m)');
subplot(3,1,2);
plot(x,2*abs(delR-delRappx)/lambda,'b');
title('error between delR and quadratic apprx to delR normalized to lambda');
ylabel('delR (m)');
axis([0 500 0 1]);
subplot(3,1,3);
plot(x,abs(delphi-delphiappx),'b');
title('error between true and ');
title('error between delphi and quadratic apprx to delphi normalized to lambda');
ylabel('delR (m)');
xlabel('cross-range (m)');
axis([0 500 0 7]);
eg4flag=1;
```

```
else
  printf("Must run eg1sar first.\n")
end
```

A.7 Code for example 4

The following code was used to generate the results for example 4.

```
% Illustrate correlation output
% Written by Yaron Seliktar
zoomflag=0;
if exist('eg4flag','var')
  % obtained from eg1
  x0 = 100; % [m] cross-range coordinate of scatterer
  R0 = Rs; % [m] range to center of footprint, we'll make it range to scattere
  % obtained from eg3
  Xtheta=thetaa*Rs; % extent of illumination at slant range
  dxt = 0.5; % increment of xt vector
  dxt = 0.1; % increment of xt vector
  if zoomflag
    xt = x0+[-5:dxt/4:5]; % zoom in
  else
    xt = 0:dxt:200; % cross-range grid at which to evaluate correlation output
  end
  idx = find(xt>x0-Xtheta/2 & xt<x0+Xtheta/2);

  a1 = xt(idx)-x0;
  a2 = Xtheta-abs(xt(idx)-x0);

  z1 = sin( (2*pi/lambda/R0)*a1.*a2 );
  z2 = (2*pi/lambda/R0)*a1*Xtheta;
  z3 = exp(-j*4*pi*R0); % phase of output
  zt = zeros(1,length(xt));
  zt(idx) = z1./z2;

  y1 = pi*sinc( (2*pi/lambda/R0)*a1.*a2/pi );
  y2 = inv(Xtheta)*a2/pi;
  yt = zeros(1,length(xt));
  yt(idx) = y1.*y2;

  clf
  %plot(xt,yt,'*');
  ylabel('y');
  if zoomflag
    plot(xt-x0,20*log10(yt));
    xlabel('x''-x0');
    axis([-5 5 -60 0]);
  else
    plot(xt,20*log10(yt));
```

```
    axis([0 200 -60 0]);
    xlabel('x''');
  end
  grid on
else
  printf("Must run eg3quadphaseerr first.\n")
end
```

Bibliography

[1] `http://www.astronautix.com/craft/magellan.htm`.

[2] William M. Brown. Synthetic aperture radar. *Aerospace and Electronic Systems, IEEE Transactions on*, AES-3(2):217–229, March 1967.

[3] William M. Brown and Leonard J. Porcello. An introduction to synthetic-aperture radar. *Spectrum, IEEE*, 6(9):52–62, Sept 1969.

[4] Walter G. Carrara, Ron S. Goodman, and Ronald M. Majewski. *Splotlight Synthetic Aperture Radar: Signal Processing Algorithms*. Artech House, 1995.

[5] J.C. Curlander and R.N. McDonough. *Synthetic Aperture Radar: Systems and Signal Processing*. John Wiley and Sons Inc., 1991.

[6] L.J. Cutrona, W.E. Vivian, E.N. Leith, and G.O. Hall. A high-resolution radar combat-surveillance system. *Military Electronics, IRE Transactions on*, MIL-5(2):127–131, April 1961.

[7] C. Elachi, T. Bicknell, R.L. Jordan, and Chialin Wu. Spaceborne synthetic-aperture imaging radars: Applications, techniques, and technology. *Proceedings of the IEEE*, 70(10):1174–1209, Oct 1982.

[8] J. Patrick Fitch. *Synthetic Aperture Radar*. Springer-Verlag, 1988.

[9] J.J. Kovaly. Radar techniques for planetary mapping with orbitting vehicle. *Anals of the New York Academy of Sciences*, 187:154–176, January 1972.

[10] John J. Kovaly. *Synthetic Aperture Radar*. Artech House, 1976.

[11] R.F. Schmidt. Radar mapping of venus from an orbiting spacecraft. In *Proceedings of the Third Symposium Remote Sensing of Environment: Infrared Physics Laboratory University of Michigan, Ann Arbor, Michigan*, pages 51–61, 1964.

[12] C.W. Sherwin, J.P. Ruina, and R.D. Rawcliffe. Some early developments in synthetic aperture radar systems. *Military Electronics, IRE Transactions on*, MIL-6(2):111–115, April 1962.

[13] Merrill I. Skolnik. *Radar Handbook*. McGraw-Hill Inc., NY, NY, second edition, 1990.

[14] C.A. Wiley. Synthetic aperture radars. *Aerospace and Electronic Systems, IEEE Transactions on*, AES-21(3):440–443, May 1985.